Various aspects of single bacterial cell:

from encapsulating nanoparticle, cell patterning and studying gene expression

by
Bum Seo

A thesis
presented to the University of Waterloo
in fulfillment of the
thesis requirement for the degree of
Master of Applied Science
in
Chemical Engineering -Nanotechnology

Waterloo, Ontario, Canada, 2016

Author's declaration

I hereby declare that I am the sole author of this thesis. This is a true copy of the thesis, including any required final revisions, as accepted by examiners. I understand that my thesis may be made electronically available to the public.

Abstract

Behaviour of single bacterium have been mysterious for many years due to the technical difficulty and nature of bacteria forming communities. It has not been long since engineers and scientists have started to develop various techniques and devices to study and isolate single bacterium. In the present thesis, three subprojects with a common theme of applying single bacterium cells for engineering application or investigating regulation of gene expressions is introduced.

Recently, metal structures with micrometer dimensions have been fabricated and successfully utilized to isolate single bacterial cells with dimensions similar to the designed pillars. First project further develops previously discovered feature of single bacterial cell isolation by metal hollow structures to capture polymeric nanoparticles inside the hollow structures. High achievement rates of filling the nanoparticles inside the structures and subsequently capping the top opening of hollow pillars have been attained. The study demonstrates that the shape of structures affects both the capturing rate and capping rate of nanoparticles.

In the second project, a fabrication method and result of simple template to obtain well organized array of single bacterial cells is shown. The bacterial cells with size less than micrometer are patterned on a gold substrate in a uniform matter. The technique developed here requires no additional binding agent nor chemical modification of the substrate which provides an advantage in saving the processing time and cost in comparison to existing techniques developed to isolate single bacterial cells. The isolated bacterial cells are further engineered with magnetic nanoparticles to illustrate bacterial cell wall property remaining the constant after deposition.

In the last project, promoter activity of single cells has been analyzed to study the population behaviour of the bacterial culture. In contrast to the assumption that the behaviour of a single bacterium would be identical as a group, the opposite behaviour was found. In the thesis, phenotypic heterogeneity within a promoter that may correlate with the external morphology is shown. During the experiment, two different morphology of cells were observed to exist in a single culture, a short cell and a long elongated cell and the promoter activity correlated with the morphology where the short body ones had higher activity in the promoter compared to the long ones. A fluorescence reporter assays are experimented and evaluated in attempt to reveal the reason behind such heterogeneity.

Acknowledgments

Thanks to my supervisors, Dr. T.Y Tsui for his continuous support and guidance throughout my masters degree. I also extend my gratitude towards Dr. I. Bischofs-Pfeifer for hosting me at the University of Heidelberg and her valuable lessons.

I thank my family for their unconditional love and support.

Thanks to my colleagues in the past and present from both Nanomechnaics of University Waterloo, Canada and Bacterial Signaling Networks of University of Heidelberg, Germany. Many have helped with their guidance and expertise in advancing the research and provided me with great memory.

I would like to thank my collaborators from Frank Gu Lab of University of Waterloo, Canada for their guidance and expertise in the area of research and speeding up the research with their help in running the experiments.

This results presented in chapter 2 of this work has also been published in journal paper ([71]).

"*To Infinity and Beyond*"
-Buzz Lightyear, Toy Story

Table of Contents

List of Figures

List of Tables

Chapter 1: Introduction

1.1 Bacteria

Ever since the microscope has been invented and first microorganisms have been seen, study and research in microorganisms have been subject to be popular. Microorganisms are diverse and may be single-celled or multicellular. They are ubiquitous and can be found to be living in every part of the biosphere. A type of single-celled organisms is a classified as prokaryote which lacks a membrane-bounded nucleus.[1] Prokaryotes can be divided into further two distinct groups called the bacteria and the archaea. A bacteria are one of the most abundant living beings in the planet and they come in diverse forms from spherical to spiral shapes.

1.2 Gram-positive and Gram-negative

Bacteria may be further differentiated into two types based on the structural differences in their cell walls. A type of bacteria which have a thick, multilayer of peptidoglycan are called Gram-positive bacteria where bacteria with single-layered bacteria are called gram-negative bacteria. The name is derived after scientist Han Christian Gram who first devised a method to differentiate two types of bacteria based on the different thickness of peptidoglycan layer. Based on the Gram reaction test, Gram-positive bacteria retain crystal violet dye and stain dark violet or purple where in contrast gram-negative bacteria can be decolourised to accept counter stain. [2]

1.3 Individual bacterial cell study

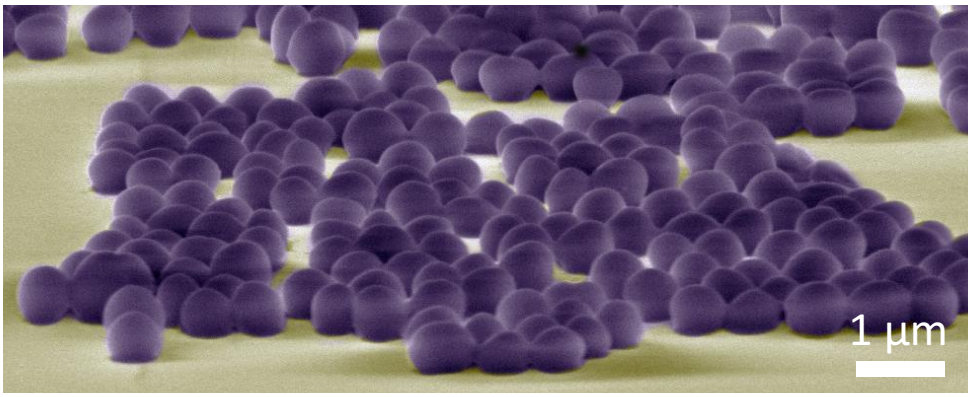

Figure 1.1 *S. aureus* bacterial cells distributed randomly on gold coated silicon substrate

Bacteria, a plural term for bacterium is much frequently used due to the fact bacteria are frequently observed as a group or in a colony. Bacteria form well-organized communities even with other species and hence studying and isolating single bacterium have long been challenged due to the technical difficulties or been ignore due to the fact that bacteria are almost never found as single bacterium. A typical image of randomly collected bacteria sample is present in Figure 1.1. As mentioned previously, isolating single bacterium and engineering it have been long been a challenge for engineers and microbiologists, recently Jahed et al. [3], have successfully observed single bacterium attachment characteristics on nickel nanostructures. This study has demonstrated that metal structures with dimensions comparable to the size of a single bacterium could be used to single cell bacterial adhesion. Inspired from this, palladium-cobalt alloy nanostructures with various cross-sectional geometries and funnel-shaped geometric features on the top surfaces have been fabricated and to study the adhesion properties of same bacteria used by Jahed et al. [3] to investigate the surface morphology effect on the adhesion characteristics of bacterial cells. [3] In order to further carry these previous researches, a characteristic of bacterial cell adhering on top surfaces of nickel nanostructures have been utilized to capture nanoparticles and is described in this thesis. In the later chapters, another method to isolate single bacterium cell without a necessary

to fabricate nanostructures is also present. An isolated bacterium is further engineered with other magnetic particles to demonstrate the possibilities of using single isolated bacterium in cleanroom fabricated devices or techniques.

Until recently microbiologist assumed that the group behaviour of bacteria would be same for all the individual bacteria that are in the colony. This assumed that all cells respond identically to the presence of stimulus to express a certain set of genes. However, questions and concerns raised as many tools have become available in the past decade. Especially with the improvement in fluorescent protein and microscope technology, it became possible to study the gene expression in the single-cell level. With analyzing the single-cell level gene expression, it was revealed that the population comprising a heterogeneous group of cells could lead to gross miscalculation with averaging the expression values. With a heterogeneous group, a gene expression is no longer a Gaussian distribution but becomes a two distinct subpopulations. In the last part of this thesis, an example of cell population heterogeneity in terms of the gene expression and the cell morphology of *B. subtilis* bacterial cell is reported.

Chapter 2: Encapsulating nanospheres inside hollow nanopillars using bacterial cells

2.1 Background on nanoparticle capturing

Micorn- and submicron particles may be functionalized by assembling organic or inorganic molecules on the surfaces or by doping these small particles. [6-10] In advanced medical drug delivery applications, these functionalized particles are utilized to deliver and release their contents to the target places. [11-15] Polystyrene, latex spheres, [7,9,11,14,18] and inorganic core/polymeric shell composites [19,22] are examples of some common nanoparticles that are widely used in tissue engineering and targeted drug delivery applications. In this part of thesis, a new method to trap two most common polymeric nanoparticles used in bioengineering field within targeted nickel hollow nanostructures with bacteria cell, *Staphylococcus aureus* (*S. aureus*) cells are presented. The nickel hollow nanostructures are fabricated on silicon substrates within simple top down fabrication method.

Up-to-this date developed fabrication method to trap or encapsulate nanoparticles are chip-based photonic devices [23] and through-silicon-via high performance integrated circuit packages. [24] In such techniques, target nanoparticles are first deposited in holes on the substrate made by plasma or wet etching. To encapsulate these nanoparticles, the opening is covered with thin films [23]. In order to deposit such thin films vacuum environment is often required. However, many biological components are known to be instable in such vacuum pressure. Different from most existing techniques, the technique presented here is a new biocompatible capping method that performs at ambient temperature and in aqueous environment.

In this work, hollow nanocrystalline (nc) nickel structures were fabricated on silicon substrates then polystyrene or latex nanoshperes were deposited in already fabricated nickel pillars. After

depositing nanoparticles in hollow structures, these particles are isolated by capping the nickel pillar opening with *S. aureus* cells. In the previous study, List of samples successfully fabricated in this work. The numbers of samples inspected during the experiments are highlighted with curve brackets. these cells demonstrated their ability to from strong biological bonds with metals within a short period of time [24-33] and therefore are chosen as a capping agent. In addition, a recent study reported by Jahed et al. [3] demonstrated capability to immobilize single *S. aurues* cells on nc-nickel pillars with C-shaped and hollow-shaped cross-sectional geometries at a success rate greater than 50%. A present method here, is a biologically friendly method which allows capping in aqueous environments and this a unique feature compare to many existing fabrication techniques required vacuum based or high temperature deposition processes. Results prove that the bonding strength between *S. aureus* and nickel arte strong enough to withstand turbulent flow stresses caused by liquid rinse process and low vacuum pressure caused by electron microscope chamber. However, possibilities to take out the deposited particle by damaging the capped cell with electron is also shown. This is believed to be the first successful attempt to confine nanoparticles within nickel nanostructures using *S. aureus* cells. The result present in this chapter have been published in a journal paper (ref. [71])

2.2 Experimental Setup

2.2.1 Nickel pillar fabrication

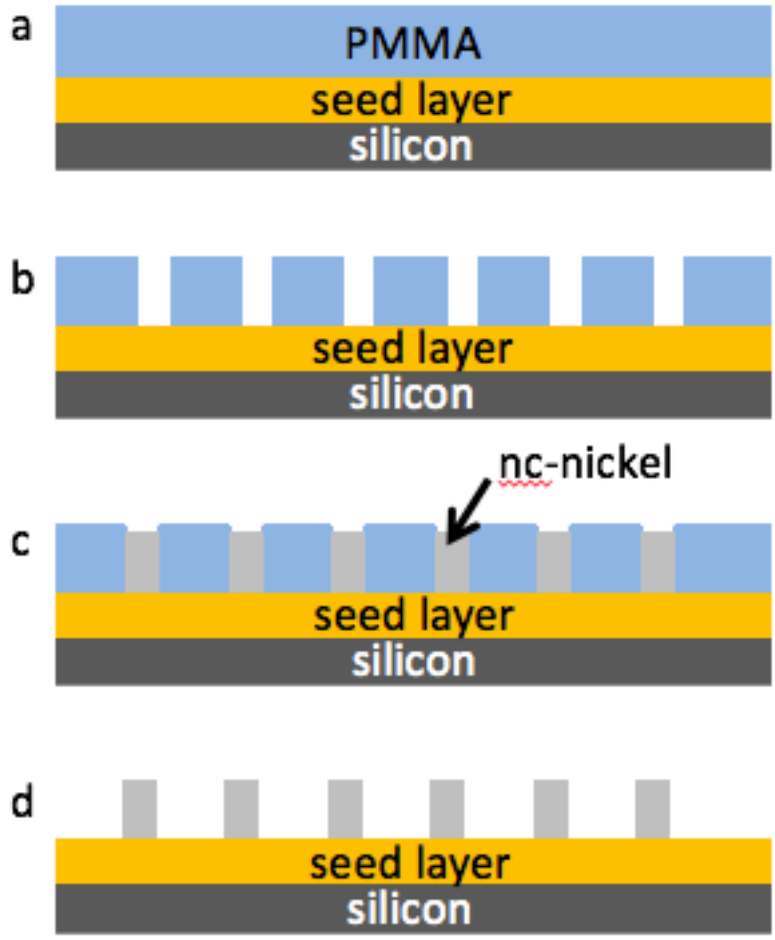

Figure 2.1 Shaped pillar fabrication procedures:

(a) spin coat PMMA on seed layer coated silicon substrates, (b) electron beam lithography, (c) plating metal into via holes, (d) acetone strip to remove PMMA

Complex geometry nickel nano pillars were fabricated on thin metal film deposited silicon substrates using electron beam lithography (EBL) and electroplating techniques following the previous published methods. [35,36]. A schematic illustration of the fabrication steps is shown in Figure 1. Briefly, seed layers consisting titanium (~20 nm) and gold (~30 - 100 nm) are deposited on silicon wafers. After the seed layer deposition, EBL photo resist, poly(methyl methacrylate)

(PMMA) is spin coated on silicon substrates with metal seed layers. Via-hole patterns were generated on the PMMA film by using a Vistec EBPG 5000+ Electron Beam Lithography System at the University of Toronto, Canada. Once the hole patterns are formed, nanocrystalline nickel electroplating deposition were conducted under ambient conditions with a direct current density of 11.5 +/- 2mA/cm^2. The exact so composition of the nickel deposition solution, Watt's bath is listed in Table 1. After the plating process, remaining PMMA resists were dissolved using acetone.

Table 2.1 Electroplating solution chemicals

Chemical	Concentration (g/L)	Purchased Company
Nickel (II) sulfate hexahydrate (99 %)	300	Sigma Aldrich
Nickel (II) chloride (98 %)	30	Sigma Aldrich
Boric Acid (BX0865)	30	BX0865, EMD Milipore
Saccharine (98 %)	1.9	Sigma Aldrich

2.2.2 Nanoparticle Deposition

Drops of nanoparticle containing solutions were applied to the pillar arrays in order to fill the metal pillar with particles. After, distilled water rinse was followed to remove an excess amount of nanoparticle solutions. Finally, specimens were gently dried with purified nitrogen. List of used nanoparticles and purchased company are summarized in the below table.

Table 2.2 List of nanoparticles used

Nanoparticle	Size (nm)	Concentration	Purchased Company
Polystyrene	~300	5% w/v	Sphereotech Inc.
Latex	~500	~1.55 x 10^{10} spheres /mL	Ted Pella Inc.

2.2.3 Bacteria culture and Deposition

S. aureus bacterial cells were inoculated on BD trypticase soy agar plates and incubated at 37 ˚C for 24 hours. Cells were harvested using 5 mL of sterilized 2.55% saline with ~0.006% nutrient broth solution and calcium alginate swabs into a sterile 15 mL centrifuge tube. The bacteria were then washed using centrifugation at 4000 rpm for 10 min. This was repeated six times for a total of seven washes. After this, the suspensions were spectrophotometrically adjusted to an optical density of 1.33 at 660 nm (OD_{660} = 1.33) using 2.55% saline. The plate counting method was used to determine the concentration value at OD_{660} = 1.33 (10^9 CFU/mL). Aseptically, the prepared live *S. aureus* was added to the patterned silicon chip such that the entire surface of substrate was covered. This was then loosely sealed within a plastic capsule to prevent significant evaporation and incubated at 37 ˚C for 1 hour. Subsequently, the surface of the chip was washed twice with 1 mL of distilled water to dislodge planktonic cells. Finally, the chip was allowed to dry at 37 ˚C for at least 8 hours.

2.2.4 Scanning Electron Microscope Inspection

To understand how effective, the polymeric spheres filled the hollow and C-shaped nanopillars and the coverage of the *S. aureus* cells on the pillar array, all of the specimens were inspected using field-emission scanning electron microscope (SEM, Zeiss 1550) after polymeric sphere introduction and the bacterial cell exposures. The accelerated voltage of the electron gun was set at 10 kV with chamber pressure below 1.5 x 10^{-5} mbar. No gold coatings were necessary for the specimens and were inspected as prepared.

2.3. Results and discussions

2.3.1 Nanopillar geometries

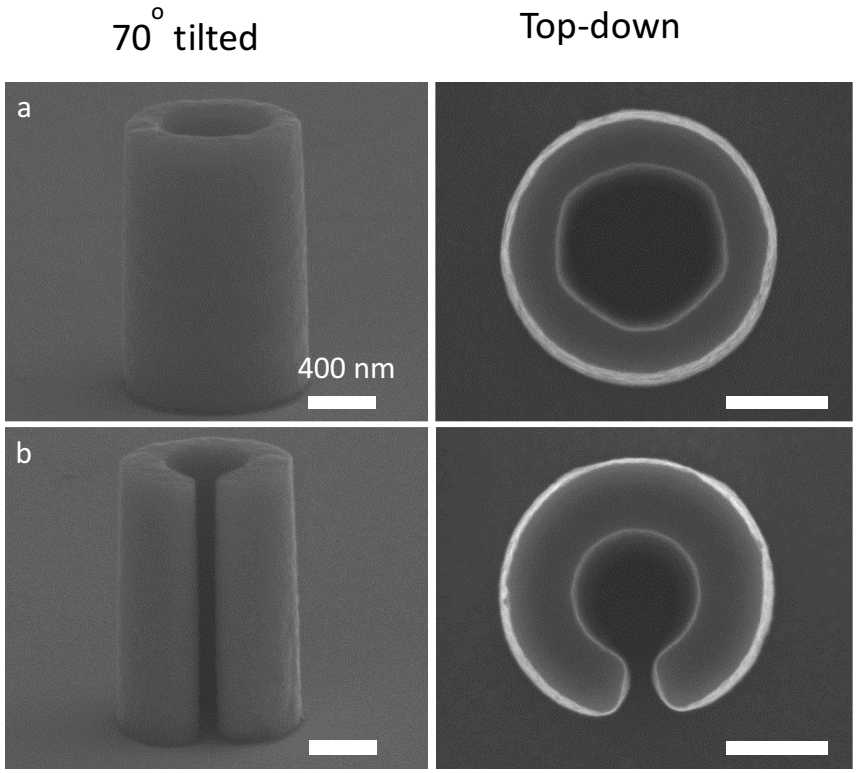

Figure 2.2 Typical SEM micrographs of as-fabricated nanocrystalline nickel pillars with (a) hollow and (b) C-shaped cross-sectional geometry. Scale bars represent 400 nm

Typical SEM images of as-fabricated nanocrystalline nickel pillars with different cross-section geometries, hollow shape and c-shaped, respectively, are presented in Figure 2.2 (a) and (b). In the previous published study, the microstructures, chemical compositions, and mechanical properties of identically prepared nanocrystalline nickel structures have been reported in detail [37]. As illustrated by SEM micrographs, the nickel pillars with an outer dimeter of 1 μm have smooth surfaces and flat tops. Top-down view of both hollow shape structures reveal no present of residue inside the structures. The detailed dimensions including the opening are summarized in

Table 2.3. Compared to C-shaped cross-sectioned geometry, hollow shaped pillars have much more wide opening. In addition to the top opening size difference, C-shaped structures have slit opening which allows exchange of surrounding environment and content of the structure.

Table 2.3 List of samples successfully fabricated in this work. The numbers of samples inspected during the experiments are highlighted with curve brackets.

Specimen	Pillar Shape	Pillar Inner Diameters (nm)	Polymeric Spheres	Particle Diameters (nm)	Particle Filling Success Rate (%)	Trapping Success Rate (%)
1	Hollow	703 +/- 21	Polystyrene	300	92 (13)	85 (13)
2	C-shaped	564 +/- 13	Polystyrene	300	64 (14)	36 (14)
3	Hollow	701 +/- 4	Latex	500	87 (39)	51 (39)
4	C-shaped	516 +/- 8	Latex	500	81 (36)	8 (36)

2.3.2 Polymeric sphere trapping effectiveness on nanopillars by *S. aureus*

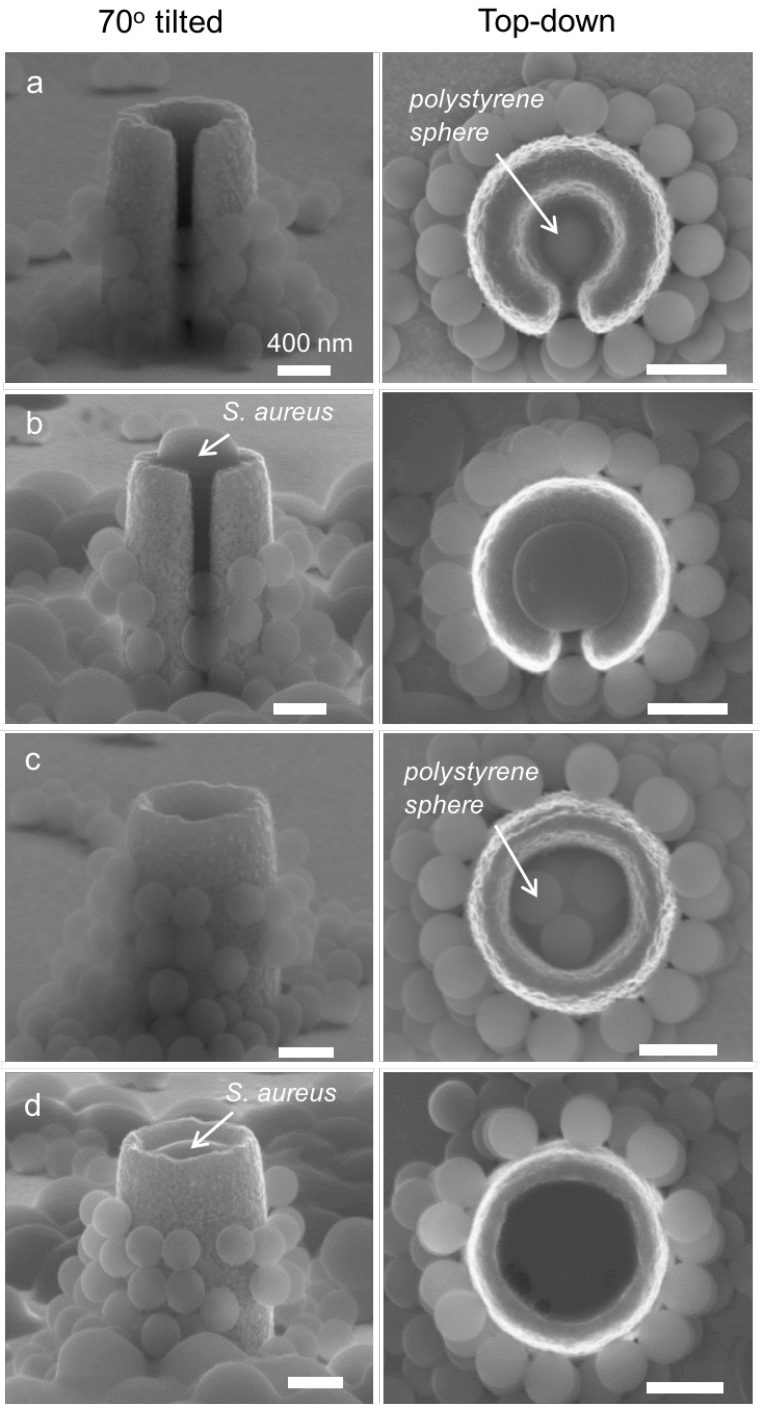

Figure 2.3 Nanocrystalline nickel pillars exposed to polystyrene spheres and then capped with *S. aureus* cells. Scale bars correspond to 400 nm

To study the trapping feasibility of polymeric spheres within nickel nanopillars, series of experiments were conducted with nanoparticles and *S. aureus* cells. Hollow shaped nanopillars

filled with polysterene or latex spheres were trapped with *S. aureus* cells. Represented SEM micrographs of polystyrene sphere filled nc-nickel C-shaped pillars obtained before and after the *S. aureus* cell deposition are displayed in Figure 2.3 (a) and 3(b). The pillar illustrated in Figure 2.3 are show a pillar before and after the cell deposition and show a single polymeric captured inside a pillar. Analysing 14 identical shaped pillars revealed that the 64 % of these pillars were successfully filled with polystyrene spheres and 36% of them were sequentially trapped with *S. aureus* cells afterward. Identical experiments with different pillar shape, hollow nanocrystalline nickel pillars were also conducted. A SEM micrograph of a hollow pillar filled with at least four polystyrene spheres is displayed in Figure 2.3(c). After exposing the same specimen to *S. aureus* cells, the SEM micrograph reveal that the top of the identical hollow pillars is successfully capped with exposed cells as shown in Figure 2.3(d). Wider openings of hollow pillars compared to C-shaped pillars (~700 vs ~550 nm) are believed to contribute to higher percentage of being filled with polymeric spheres. 85% of inspected C-shaped pillars were filled with polymeric spheres while 92% of hollow structures were filled with particles.

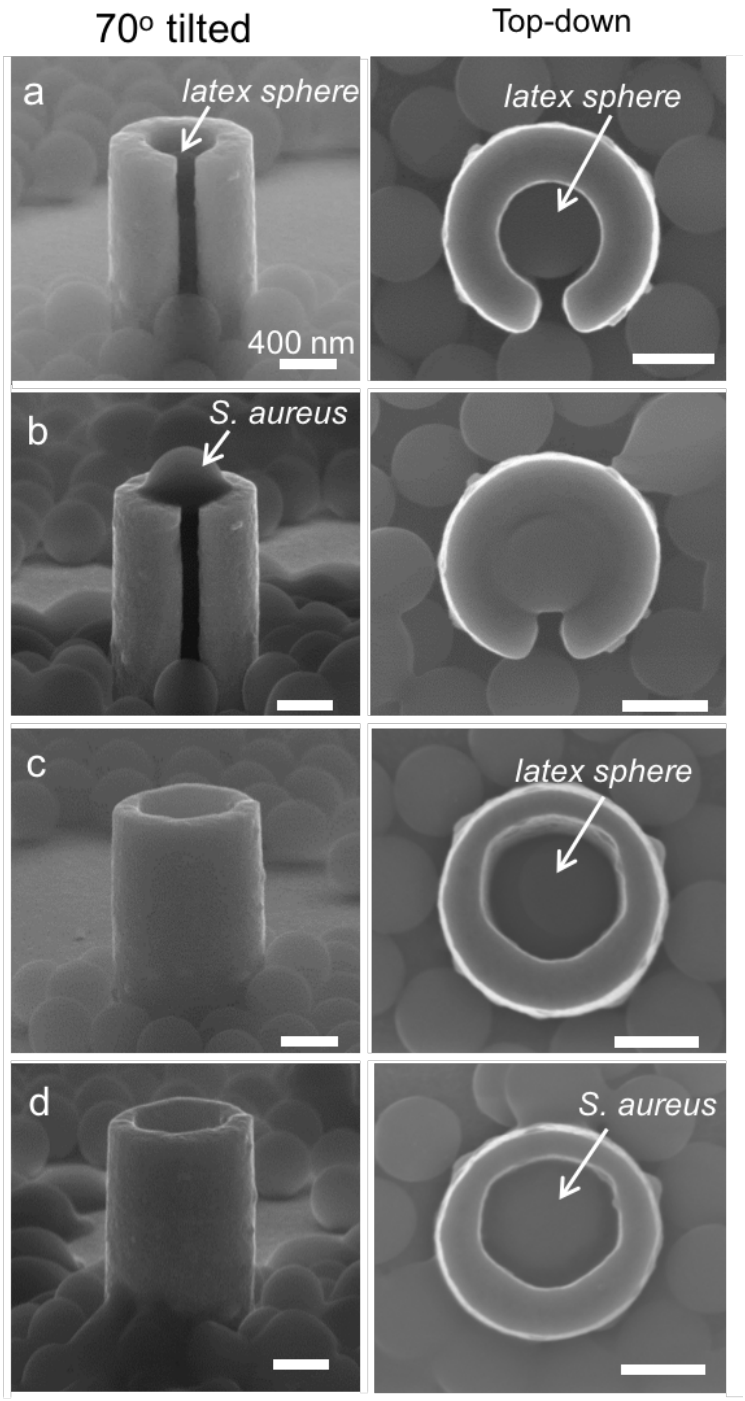

Figure 2.4 Nanocrystalline nickel pillars exposed to latex spheres and then followed with *S. aureus* cells. Scale bars correspond to 400 nm

In order to demonstrate possibility of encapsulating versatile polymer spheres and to compare the size effect of polymer spheres, similar experiments were performed with latex spheres which had a diameter of ~500 nm on hollow and C-shaped nickel pillars as shown in Figure 2.4(a)-(d). These

micrographs clearly show that the presented method can be applied to different polymeric sphere materials and different particles sizes as long as its smaller than the openings of hollow and C-shaped pillars. Figure 2.4(a) reveal typical tilted and top-down micrograph of a nc-nickel pillar containing latex spheres. Exact same pillar with a *S. aureus* cell adhere on top opening and sealing the top at the same time are shown in Figure 2.4(b). The success rate of these two processes, filling with latex spheres and capping with *S. aureus* cells were 81% and 8% respectively. The low capping rate of 8% may be due to overfilling of the latex spheres in some of the pillars. An example of a pillar overfilled with latex spheres is presented in Figure 2.5. A protruding latex sphere beyond the top of the pillar surface may potentially hinder *S. aureus* cells from attaching on the pillar top. Experiments were also successfully conducted with hollow nc-nickel pillars and latex spheres, and the results are presented in Figure 2.4(c) and 2.4(d). The presented micrographs reveal that latex spheres can also be deposited in the hollow structures similar to C-shaped pillars and that both shaped pillars can be capped with *S. aureus* bacteria cells to cover the top surface. The success rate of hollow pillars was 87% and 51% respectively. The summarized result is presented in Table 2.3. This table clearly illustrates the versatility and potential of this method based on the simple method and parameters, interior dimeter of the pillars to deposit and trap polymeric particles using bacterial cells.

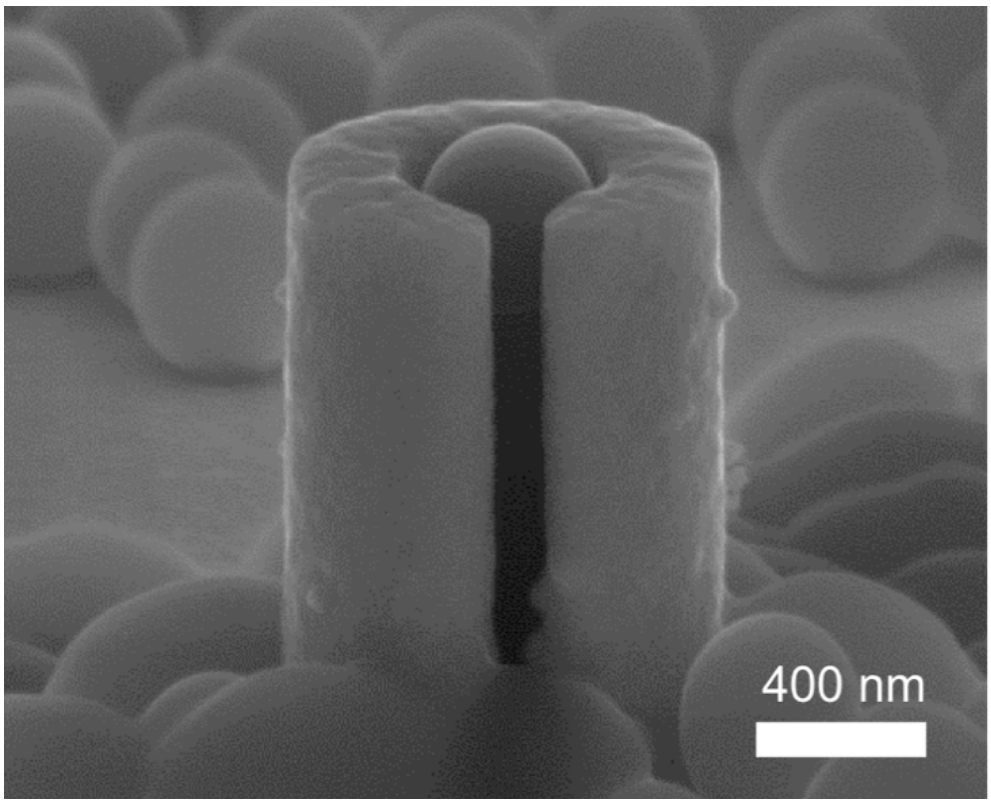

Figure 2.5 C-shaped nanocrystalline nickel pillar with latex sphere protruded beyond the top surface

2.3.3 *S. aureus* bacterial cell capping reliability

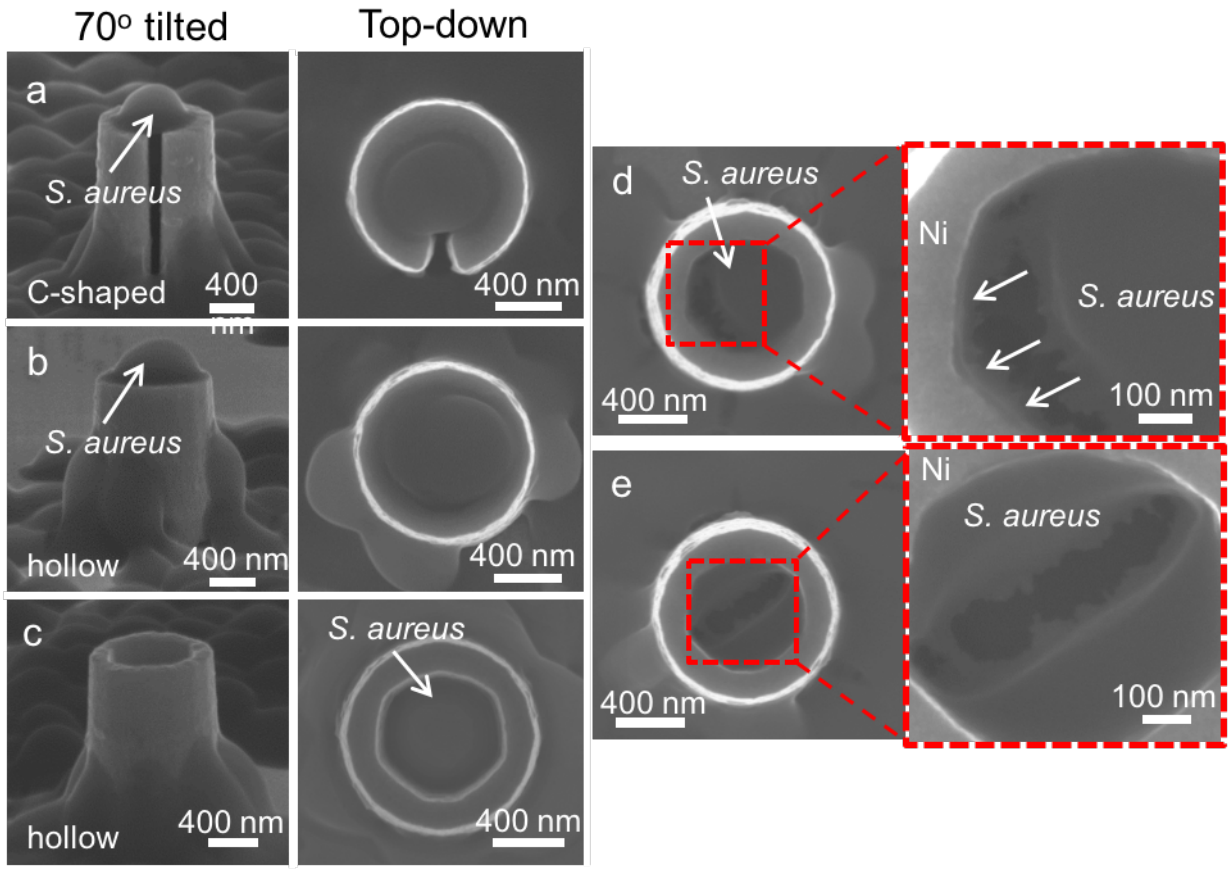

Figure 2.6 *S. aureus* bacterial cells attached to (a) C-shaped and (b)-(c) hollow nc-nickel pillars. *S. aureus* bacterial cells ruptured during the SEM imaging process (d) near the sidewall of the pillar and (e) at the middle of the cells.

SEM inspection of the post bacteria exposed pillars reveal that the *S. aureus* cells attach to different locations of C-shaped and hollow shaped pillars. Among inspected C-shaped pillars, there was not a single C-shaped pillars where the micro-organisms have entered the interior of these structures, *S. aureus* have only adhered on the top surfaces of the C-shaped pillars. Differently, with hollow pillars *S. aureus* showed ability to attach on the top surfaces or enter the interior. If cells fall into the interior space of hollow shaped pillars, the cells adhered to the sidewalls. The different adhering characteristics of cells were also observed on specimens without polymer spheres deposited inside the metal pillars as shown in Figure 2.6(a)-(c). The different inner diameters between C-shaped shapes (~550 nm) and hollow shaped (~700 nm) pillars may contribute to the

different attachment behaviour of cells. The top opening of C-shaped pillars is considerably smaller than the diameter of *S. aureus* bacterial cell which prevented them from entering the interior of the structures. In comparison, the inner opening of hollow pillars is significantly larger which *S. aureus* cells have no problem entering the interior space.

The adhesion strength, reliability, of *S. aureus* cells to fabricated pillars were studied by exposing the attached cells with an electron beam. Once they have been irradiated with an electron beam, cells showed shrinkage which caused tensile stress on the bacteria cell wall eventually causing fracture and partial detachment between micro-organism and metal pillars. In most cases, the detachment induced from the electron beam damage was observed near the interface between the cells and the metal pillar sidewalls as shown in Figure 2.6(d). This figure shows a *S. aureus* cell adhered on hollow pillar and after exposing a cell for ~7 minutes with electron beam at a voltage value of 10 kv. The wide opening between the cell membrane and sidewall of nickel pillar is observed. It is important to note that the total exposed value may not be exactly 10 kv since exact exposed area of electron beam is unknown. The cell membrane started rupturing after only ~1 minute of exposure and the opening gradually increased with exposure time. Higher magnification inspection of the damaged area revealed that the fractures occur cohesively at the cell wall. Figure 2.6(d) also show residual material from the cell walls still remain attached to the pillar after the rupture and the they are noted by arrows in the same micrograph. The evidence of residual material indicated that the adhesive strength or the interfacial strength between the *S. aureus* and nickel are stronger than the cohesive strength of the cell walls in the vacuum environment. Another example of damaged cell wall membrane from electron beam is presented in Figure 2.6(e). The second example presented in Figure 2.6(e) is an example of cell wall damage induced by ~10 minutes of electron beam exposure of a bacteria cell adhere on the interior opening of a hollow pillar. Similar

to the previous example, the initiation of rupture was overserved after ~ 1 minute electron beam exposure. Different from the another example shown at Figure 2.6(d), the cell wall rupture was located at the middle of the bacteria while the rest of the cell wall remained attached to the metal pillar sidewall. This is another indication that the cohesive strength of cell wall is weaker than the binding strength between the cell wall and metal, nickel. The cell wall damage was only observed within hollow pillars and not observed for the C-shaped specimens even under the same electron beam exposure time. The attempt to rupture the cell wall with longer exposure time and even with electron beam operating at higher accelerating voltage failed to rupture cells adhere on C-shaped pillars. The longest exposure time attempted was 20 minutes. It is unclear whether cells on the C-shaped pillars will rupture with an increased period of exposure time or with higher strength of electron beam. The exact mechanism leading to different behaviour of cell wall rupture depending on the specimen shape still remains to be elucidated. The different adhesion locus of cell on nickel pillars could be a possible reason for such behaviour. From the inspection, it was shown that the *S. aureus* cells tend to adhere on top of the C-shaped pillars rather than within the inside of the opening as the hollow structures. The result from this study suggest that in order to obtain a reliable coverage that can resist damage from the electron beam, the pillar inner dimeters should be smaller than the dimension of the *S. aureus* cells identical to the C-shaped structures. In this case, the adhered cells are less likely to be damaged.

2.4 Conclusions and future recommendation

In this part of the thesis, new technique to fill hollow shaped nanocrystalline nickel pillars with submicron polymeric spheres and to seal the top opening of specimens with live gram positive bacterial cells, *S. aureus* was presented. All tested specimens were carefully examined with field emission scanning electron microscope. The result from the presented section indicate that bacterial cells are able to cover and seal the top opening of the structures when the inner opening diameter of the structure is smaller than the micro-organism itself. Conversely, tested micro-organisms entered the interior opening of the pillar when the cell size was smaller than structure opening. The success rate of depositing polymer spheres and capping the pillars improved with inner opening diameters. Overall, the highest results were shown with the hollow pillar which had the largest diameter among tested specimens with ~703 nm. Both filling and cell trapping rate of polystyrene spheres were highest with hollow pillars with a success rate of 85 % or better.

The presented project could be carried forward by testing capping potential of other shaped bacteria. In the presented study, only spherical shaped ones were used, however it is recommended to use other micro-organism such as *E. coli, B. subtilis* which have more elongated shapes to see whether the capping success rate changes or not.

Chapter 3. Bacterial cell patterning on gold-coated silicon substrates

3.1 Background on single cell patterning

Various methods for immobilizing bacterial cells have been developed and studied in the last few years. One of the prominent challenges that arise in immobilizing a bacterial cell is the isolation of the cell in a controlled manner. A technique capable of controlling bacterial adhesion and patterning makes investigating biological phenomena within a cell possible, as most cell studies currently rely on statistical distributions based on populations of cells. In addition, the ability to position cells on a surface in a desired arrangement or manner, also known as cellular patterning, is a potential method to study and monitor cell-to-cell, intracellular, and extracellular interactions [39-42]. Previously explored techniques for immobilizing microorganisms in a randomized manner include using electrostatic [43], chemically modified surfaces [44], or mechanical trapping [45]. Current common methods of organizing individual or multiple cells include MicroContact printing (μCP) [46-48], microfluidics [49], inkjet printing [50], stencils [51], and robotics [52]. However, many previously fabricated patterns have pattern dimensions greater than several micrometers, which eliminate the possibility of analysing numerous smaller, submicron bacterial cells. Moreover, many explored techniques use anti-adhesive agents to separate the cell colonies from the stamp to the substrate [41]. Immobilizing single microorganisms in ordered patterns have always been the prerequisite for testing mechanical properties of both living and dead cells. In order to study Young's modulus of living and dead *Escherichia coli* via atomic force microscopy (AFM) indentation experimentations, Cerf et al. [48][53] have fabricated highly ordered arrays of *E. coli* via chemical patterning. This was done using MicroContact printing (μCP) soft lithography of octadecyltrichlorosi (OTS). However, work by Cerf et al. [48][53] showed that the functionalizing agent streptavidin formed an unexpected 10 μm wide "M" shaped pattern, which

is postulated to be caused by capillary effects. This pattern might be successful for immobilizing and isolating rod-shaped bacterium cells such as *E. coli,* but it would be difficult to obtain the identical result using the same methodology for spherical cells such as *Staphylococcus aureus*. *S. aureus* is a pathogenic bacterium that is spherical in nature, and has diameters of approximately 0.5 μm. This particular strain of bacteria is known to adhere to both organic [54][55] and metal surfaces [54,56-58] . In the presented work, an array of single *S. aureus* has been successfully patterned from a PMMA mold, with *S. aureus* interfaced with gold nanoparticles and magnetic iron oxide particles. Various fields such as biophysics, biochemistry, and biomedicine can benefit from the ability to arrange submicron single bacterium in precise desired patterns. The combination of bacterium with nanoparticles suggests the possibility of applying these units as basic building blocks or platforms for enhancing biological nanotechnology.

3.2 Experimental Setup

3.2.1 Materials

Table 3.1 List of chemicals used

Compound	Purchased from
Gold (III) chloride hydrate (HAuCl4•xH2O)	Sigma-Aldrich (Oakville, ON, Canada)
Cetyltrimethylammonium bromide (CTAB	Sigma-Aldrich (Oakville, ON, Canada)
Sodium borohydride	Sigma-Aldrich (Oakville, ON, Canada)
Silver nitrate	Sigma-Aldrich (Oakville, ON, Canada)
L-ascorbic acid	Sigma-Aldrich (Oakville, ON, Canada)
$FeCl_3 \cdot 6H_2O$ (≥99%, puriss. p.a., Reag. Ph. Eur.)	Sigma-Aldrich (Oakville, ON, Canada)
Ammonium hydroxide (28% NH_3 basis, ACS grade)	Sigma-Aldrich (Oakville, ON, Canada)
Poly(diallyldimethylammonium chloride) (PDADMAC, 100-200 kDa, 20% in H_2O)	Sigma-Aldrich (Oakville, ON, Canada)
Poly(sodium 4-styrenesulfonate) (PSS, 70 kDa)	Sigma-Aldrich (Oakville, ON, Canada)
25% glutaraldehyde solution (electron microscopy grade)	Sigma-Aldrich (Oakville, ON, Canada)
Trisodium citrate dihydrate	Thermo Fisher Scientific (Burlington, ON, Canada)

Strain / Chemical	Purchased from
S. aureus (ATCC 6538)	Cedarlane Labs (Burlington, ON, Canada)
BD trypticase soy agar (TSA) culture plates	VWR (Mississauga, ON, Canada)
BD nutrient broth	VWR (Mississauga, ON, Canada)
Sodium chloride (ACS grade)	VWR (Mississauga, ON, Canada)
Nalgene sterilization filter units	VWR (Mississauga, ON, Canada)
Calcium alginate swabs	VWR (Mississauga, ON, Canada)

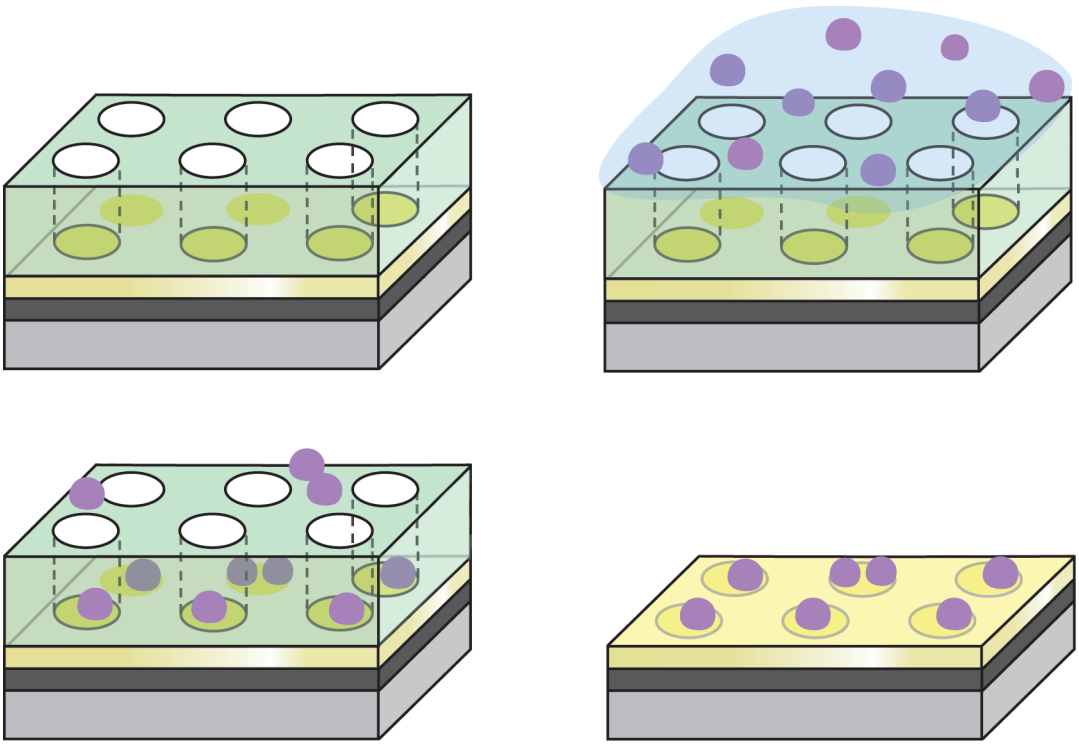

Figure 3.1 Schematic design process to fabricate ordered arrays of bacterial cells.

(a) Patterned structure of PMMA resist with ebeam lithography (b) diluted solution of bacterial cells on the PMMA mold (c) Adhesion of bacterial cell on gold substrate and PMMA surface (d) PMMA resist removal via acetone

3.2.2 PMMA Template Fabrication

Submicron holes were manufactured using electron beam lithography (Figure 3.1) to immobilize and isolate *S. aureus* cells. A thin layer of titanium (~20 nm) and gold (~100 nm) film were first deposited on silicon substrates via electron beam deposition. The silicon substrate with overlaying layers of titanium and gold were then spin coated with Poly (methyl methacrylate) (PMMA) EBL resists. Finally, holes with a diameter of 1 μm were created on these silicon wafers by exposing the films to a beam of electron.

3.2.3 Bacteria culture and Deposition

S. aureus was cultured on trypticase soy agar (TSA) plates overnight at 37 ºC. A 2.55% saline solution was prepared and sterilized using Nalgene filters, and 0.006% nutrient broth was added to preserve *S. aureus* during the testing period. *S. aureus* cells were transferred to saline solution by adding 5 mL of saline to the TSA plates, and alginate swabs were used to dislodge the bacteria from the plates. *S. aureus* cells were washed with saline solution once by centrifugation at 4000 rpm for 10 minutes. The washed solution was normalized to optical density at 660 nm (OD_{660}) of 1.0 ± 0.1 (10^9 CFU/mL [59]).

During a typical test, a drop of OD_{660} normalized *S. aureus* solution is placed on the silicon substrate containing submicron sized holes. The specimens were placed on a Stovall Life Science Inc. (Peosta, IA, USA) Belly Dancer orbital shaker for one hour at room temperature. The bacteria are then cross-linked with a 2.5% glutaraldehyde solution at room temperature for one hour. The excess solution of glutaraldehyde is extracted and the sample is washed with deionized water twice. The samples are then dried overnight in the incubator at 37 ºC. In order to isolate the array of single *S. aureus* cells, the PMMA mold was stripped off in acetone. *S. aureus* cells that had adhered to the top of the PMMA structure were removed simultaneously along with the mold itself, and hence a controlled assembly of bacteria was created (Figure 3.1).

3.2.4 Nanoparticle Deposition

3.2.4.1 Gold Nanoparticles

Cationic surfactant-coated gold nanoparticles were synthesized according to previously published procedure [60]. Briefly, the gold nanoseed was first synthesized by adding 60 μL of 0.1 M freshly prepared ice-cold sodium borohydride to 20 mL of a gold (III) chloride hydrate (2.4×10^{-4} M) and

trisodium citrate dihydrate (10^{-4} M) solution under vigorous stirring. The sample was incubated overnight in the dark in ambient conditions, filtered (0.2 μm) and stored at 4 °C until use. To synthesize cationic gold nanoparticles, cetyltrimethylammonium bromide (CTAB) was used as a negative template. Gold (III) chloride hydrate (8.97 mL, 11 mM) and silver nitrate (0.67 mL, 10 mM) were added to 210 mL of 1.46 mM CTAB solution under moderate stirring. Then, L-ascorbic acid (1.44 mL, 100 mM) was added drop-wise and the solution turned clear. Then, 5.60 mL of gold nanoseed was immediately added. The nanoparticles were purified by centrifugation at 10,000 rpm for 15 min resuspended in 1 mM CTAB solution. In order to deposit these nanoparticles, a drop of gold nanoparticle solution was added to the silicon substrate after a one-hour incubation period of the bacteria. The nanoparticle solution was incubated with the bacteria for 15 minutes on the orbital shaker. The excess bacteria and particles were extracted. The bacteria were cross-linked with glutaraldehyde for one hour and then washed with deionized water twice, followed by drying, and removal of PMMA.

3.2.4.2 Iron Oxide magnetic particle

Spindle shaped hematite iron oxide particles were synthesized according to a previously established protocol [61], using a NaH_2PO_4 concentration of 0.2 mM. The iron oxide particles were subsequently coated with a shell of amorphous silica according to a modified Stöber process [62][63]. The silica-coated particles were then reduced under flowing H_2 gas (100 cm^3/min of 50% H_2 in Ar for 6 h at 350 °C) in a tube furnace to convert the iron oxide in the core to magnetite. The particle surface was then functionalized with poly (sodium 4-styrenesulfonate) (PSS) to impart a permanent negative charge, according to the layer-by-layer (LbL) process [64][65]. Briefly, PDADMAC and PSS were sequentially coated onto the particles in alternating layers, beginning with PDADMAC and terminating with PSS (4 polymer layers in total). The particles were then

diluted to form a 1 g/L suspension in deionized water.

Deposition of iron oxide magnetic nanoparticles was performed after the deposition of gold nanoparticles. First, the excess gold nanoparticle solution was extracted and the sample was rinsed once with deionized water. Then, a drop of magnetic nanoparticle solution was added and incubated with the sample at room temperature for 15 minutes on the orbital shaker. The excess solution was extracted and bacteria were cross-linked with glutaraldehyde for one hour. This was followed by washing with deionized water twice, drying, and PMMA removal.

3.2.5 SEM Characterization techniques

A field emission scanning electron beam microscope (Zeiss LEO 1550 SEM) was used to inspect the immobilized *S. aureus* cells. All images were taken at a 70º SEM stage tilt. In-lens SE and SE2 detectors with an accelerating voltage set at 10 kV were the parameters used to image the sample

3.3 Results and Discussion

3.3.1 Single bacterial cell isolation and patterning

The scanning electron microscopy (SEM) image of a single *S. aureus* cell array achieved by EBL and PMMA mold is shown in Figure 3.2 (a). By the fine-tuning of EBL, distances of 10 μm between immobilized cells were achieved. Given that the holes fabricated via EBL were approximately 1 μm in diameter, only one or at most two cells (each cell with a diameter of ~0.5 μm) were able to fit into these openings. The SEM images of single and double *S. aureus* cells are represented in Figure 3.2 (b) and (c) respectively. The binding sites between *S. aureus* cells and gold substrate are clearly defined by the contrast in the SEM images. It is unclear whether the cells shown in Figure 3.2 (c) are two cells which fit into one hole, or a fallen stack of two *S. aureus* cells originally lying on top of each other. The success rate for the adhesion and immobilization of bacterial cells on the gold substrate holes made by EBL was quantified and to be 86 ± 2 %. The data spread corresponds to one standard error. At least 200 data points were considered for analyzing the success rate. Among these, ~98 % had a single *S. aureus* bacterium isolated and ~2 % of the total examined population had two or more cells isolated. Prior to removal of the PMMA mold, some *S. aureus* cells were adhered onto the PMMA surface. *S. aureus* adhesion to various polymers including PMMA has been previously observed and investigated in the past [55][67]. Due to the widespread usage of PMMA in securing bone implants in situ, PMMA-based terpolymers that prevent *S. aureus* adhesion have been designed and synthesized by Angnostou et al. [68] Such PMMA-based terpolymers can be associated with our method to study the areas where cell population is crucial, such as quorum sensing. A plausible limitation that arises from the procedure is the possibility of cell wall modification when the PMMA template is being removed via acetone. To overcome this challenge, a process to remove the PMMA mold while

avoiding damage or causing the death of the cell is under development at present time.

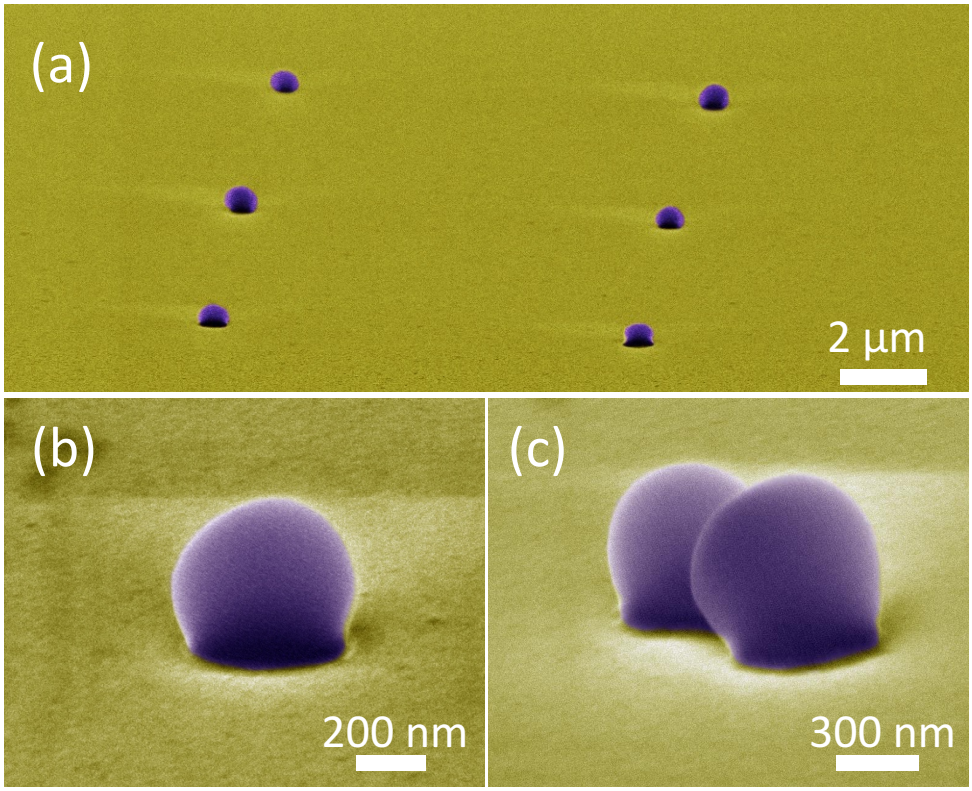

Figure 3.2 Representative false-colored SEM micrographs revealing immobilized and isolated *S. aureus* cells.

(a) a highly ordered array of single *S. aureus* cells (b) one single *S. aureus* cell (c) two *S. aureus* cells side by side

3.3.2 Engineering isolated bacterial cell with nanoparticles

As a further step in developing the introduced method, different types of nanoparticles including gold and iron oxide have been engineered with *S. aureus* cells and are represented in Figure 3.3 (a) and Figure 3.3(b). Gold nanoparticles have a positive surface charge because of CTAB coating and will aggregate around bacteria because of the negatively charged cell wall [59][60]. Gram-positive bacteria such as *S. aureus* are known to have a negatively charged cell wall due to the presence of negatively charged teichoic acids linked to either the peptidoglycan or the underlying plasma membrane [66]. The nanoparticles were deposited prior to stripping the PMMA. As a result,

isolated single cells or two smaller than average size bacterial cells were able to interact with nanoparticles inside the holes. The ability for bacteria cells to interface with particles demonstrates continuous functionality in cell walls even after the cells have adhered to the gold substrate, as it has been demonstrated before that CTAB-coated gold nanoparticles require a polyanionic surface to aggregate around bacteria [60]. This suggests a possible use of the bacterial array for modification with *S. aureus* specific biomolecules such as antibodies [69] or aptamers [70]. The magnetic iron oxide nanoparticles have a negative charge because of their polymer coating and are hence, attracted to the gold nanoparticles. Besides the gold nanoparticles and *S. aureus*, the magnetic particles were also adhering to the gold substrate. Figure 3.33(b) shows a SEM image of single *S. aureus* bacterium with gold nanoparticles and iron oxide. The magnetic iron oxide particles on top of and surrounding the cells are orientated such that they cover the largest surface area where the gold nanoparticles adhere to the cell. A columnar structure of *S. aureus* with gold and iron oxide particles is presented in Fig. 3.3c). The columnar structure has a dimension that is greater than a single *S. aureus* bacterium with the surrounding particles taken into account. Since the bacterial cells were deposited prior to the particles, it can be easily concluded that the presented figure is a result of two layers of *S. aureus* cells being supported by gold and magnetic iron oxide particles. Fig. 3d) shows two *S. aureus* bacterial cells integrated with gold nanoparticles and iron oxide magnetic particles. The presented image demonstrates that magnetic iron oxide particles can combine solely with gold nanoparticles and adhere to the cell membrane. It also establishes that the iron oxide particles can attach to the gold particles independently without any mechanical support from the gold substrate. The engineered interface between the bacterial cell and layers of charged particles demonstrates the possible use of the presented technique as a basic building block for interfacing bacteria with microsystems where the method is fully compatible with standard

micro/nano fabrication techniques.

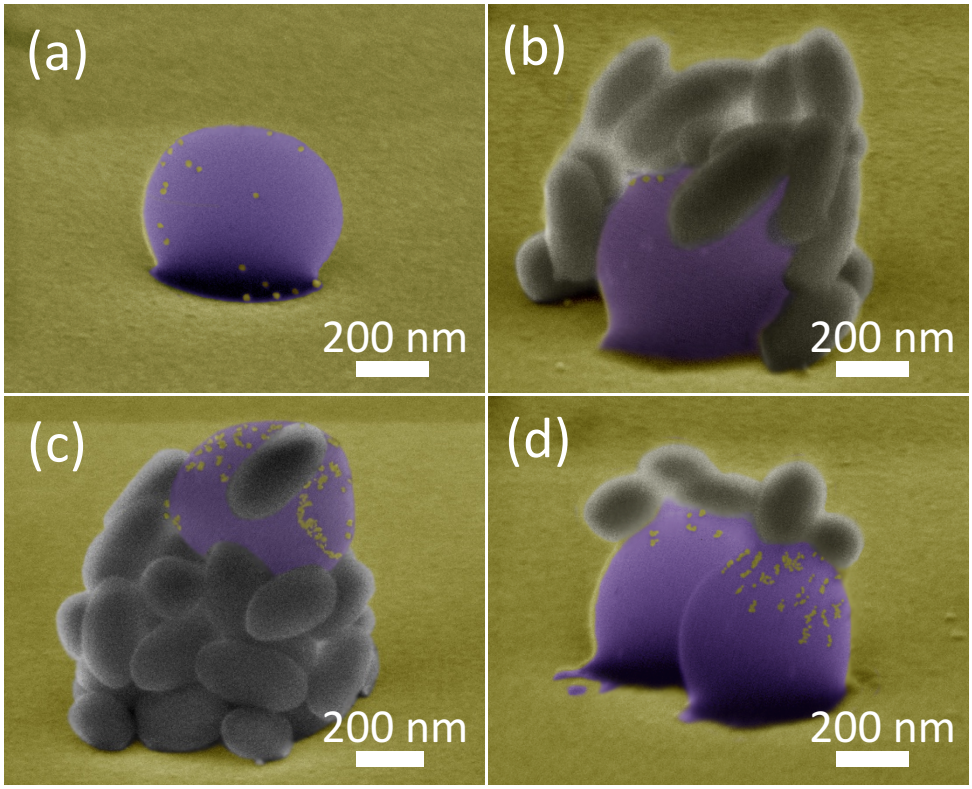

Figure 3.3 False-colored SEM micrographs of engineered cells with (a) gold nanoparticles (b) – (d) gold nanoparticles and iron oxide particles

3.4 Conclusions and Future Recommendations

A highly ordered planar array of single submicron bacterium is obtained using an engineered pattern fabricated via simple EBL technique. To avoid any artificial changes in the bacteria, surface modifying or binding agents are not used in this method. The immobilization of *S. aureus* bacterium is achieved via creating the metallic surface with selected areas covered by the EBL photoresist template, which is easily removable for the purpose of isolating the bacterium. This method can be widely adopted to fabricate arrays of various microorganisms by simply changing the dimensions of the template. In addition, sustainability of cell wall functionality after the isolation and adhesion of the cells onto the substrate has been proved by interfacing the bacterium with submicron particles utilizing electrostatic properties.

Chapter 4. Phenotypic Heterogeneity in undomesticated *B. subtilis*

4.1 Background

4.1.1 Bacillus subtilis (*B. subtilis*)

Bacillus subtilis (*B. subtilis*) is a gram-positive bacterium that is traditionally viewed to be grown only in soil, however recent investigations have discovered they are ubiquitous bacteria which can be found not only in soils but in guts of animals as well as in sandy soil. [72] *B. subtilis* is widely known for its ability to adapt to harsh conditions by becoming metabolically inactive spores under nutrient limited conditions and endure extreme environmental conditions. [73] Identical to all members of genus Bacillus, *B. subtilis* is a rod-shaped bacterium that typically forms small clumps, chains, or single cells. It is one of the most widely studied Gram-positive bacteria. A most widely used strain of *B. subtilis* is a laboratory strain 168. However, it has been found that the typical laboratory strain 168 differs from wild type strain due to genomic shift and cannot produce some specific proteins. In this study, a wild type strain (undomesticated strain), PS216 is used. This strain is isolated from sandy soil sample near River Sava, Slovenia and still has variety of important phenotypes that have been lost in the domesticated strain such as 168. [74]

4.1.2 Phenotypic Heterogeneity

Until recently, variation among individual microorganisms have been believed to be mainly due to genetic differences and environmental influences. However, many studies have reported variant in cellular functions, and morphology among genetically uniform bacterial cells that have been grown in identical environment. The diverse expression patterns between genetically identical individual cells that live in the same environment is termed phenotypic heterogeneity. Observations of phenotypic heterogeneity in various microorganisms have altered

traditional view of assuming genetically identical bacteria as homogeneous sample. Microorganisms such as bacteria may benefit from phenotypic heterogeneity when adapting to its always fluctuating surroundings.[75] In previous published results, *B. subtilis* showed phenotypic heterogeneity under nutrient limited conditions where about half of the cell population produced master regulator for sporulation while the remainder did not. [76-78] There are many other examples of population heterogeneity with *B. subtilis* during different stages of its life cycle. For instance, during the exponential phase of growth, two distinct subpopulations in terms of both the gene expression and morphology have been reported to coexist. One type had a morphology of short single swimming cells with the active transcription factor for motility while the other type showed long chains of sessile cells. [78]

4.1.3 Gene expression

4.1.3.1 Surfactin & Pectin Lyase

Surfactin is a bacterial cyclic lipopeptide that is produced by various strains of *B. subtilis*. Being a biosurfactants, it has a property to reduce surface tension of water at low concentrations. It has been reported that at concentration as low as 0.005 %, the surface tension of water has reduced from 72 to 27 mN/m. With decreased surface tension of water, *B. subtilis* can swarm easier and benefit from this in terms of the motility. At a higher concentration it is consider to be an effective antibiotic with an ability to penetrate the cell membranes of both Gram-negative and Gram-positive types of bacteria. In *B. subtilis*, srf gene encodes for the surfactin synthetase protein. [79] Pectate lyases also known as pectate transeliminases and its role is to breaks down a cell walls of many plants by eliminating cleavage major component of the primary plant cell walls, de-esterified pectin. Pectate lyases have been found to be secreted by many plant pathogenic bacteria including

B. *subtilis*. Breaking down plant cell wall is also related to fruit softening and modifications of the pectin lyases fraction are some of the most apparent changes that take place in the cell wall during ripening. [81]

4.1.3.2 ComX Signalling

Like many other bacteria, cell-cell signalling process is one of a communication method for *B. subtilis*. [82] A bacterial cell-cell communication process that regulates the gene expression depending on the bacterial population density is termed quorum sensing. [83] ComX signalling pathway is one of a known quorum sensing pathway for *B. subtilis*. It is known to control more than 10% of genome wide gene expression. [84] The flow diagram showing the mechanism of ComX signalling pathway is presented in Figure 4.1. As a first step, inactive precursor peptide called preComX is produced inside a cell. This peptide is released as ComX into the environment after being modified by ComQ with a process called farnesylation. [85] With increasing the cell population, the concentration of ComX signal increases accordingly outside of the cells. Once a threshold concentration is reached, a receptor histidine kinases called ComP detects ComX signalling molecules. ComP then autophosphorylates upon binding to ComX and ComP phosphorylates to the downstream transcriptional activator ComA, becoming ComA~P. ComA~P now has an increased affinity to bind to the promoter region eventually driving the transcription of different gens. While phosphorylating increases the affinity to bind, there are other that may sequester from binding to the promoter region. ComA or ComA~P may be blocked by other proteins which are also regulated by identical signaling pathways to ComX signalling pathways (cell-cell signaling pathways). [86] These sequester proteins such as RapC, RapF and RapH is known to inhibit the DNA binding of both ComA and ComA~P. By doing so, ComA controlled genes could be down regulated without interfering the phosphorylation of ComA.

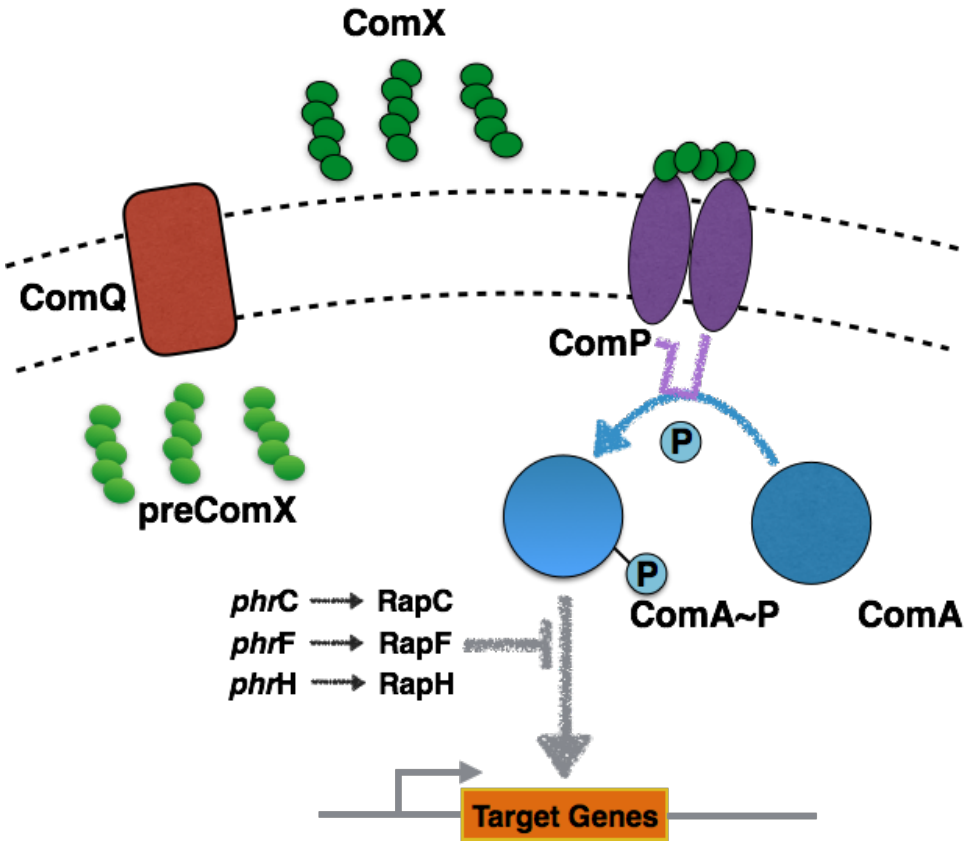

Figure 4.1 ComX signaling pathway

4.1.3.3 The Common Transcription Factor ComA

ComA is a transcription factor protein consisting two major components. ComA transcription factor is known to regulate genetic competence and quorum sensing in *B. subtilis*. ComA activates transcription by binding to recognition elements (RE) in bacterial promoters. [87] The binding sites of ComA are explained in more detail later on. Both examined promoters in this study, P*pel* and P*srf*, are known to be regulated by ComA. [88]

4.1.3.4 ComA Binding Motif

ComA is believed to be a transcription factor that mediates global changes in gene expression in *B. subtilis* and about 20 genes are found to be under its direct control. The promoter sequences of

these genes controlled by ComA consist of two recognition elements. These ComA binding motifs are called Inverted Repeat (IR) together. The two elements which make up the IR are consist of a specific ComA binding motif which another one is an inverted complement of the first one. In addition to these two recognition elements, recent study has found two additional ones which are together called the Direct Repeat (DR). Both IR and DR have been identified in-vitro as ComA binding sites. By comparing several wild-type promoter constructs of ComA binding sites, an idealized motif for the IR and DR was derived. These synthetic promoters contain a combinations of perfect direct repeats (PDR) and perfect inverted repeats (PIR). The sequence of natural promoters investigated here and synthetic promoters constructed in the previous study are listed below obtained from ref [89].

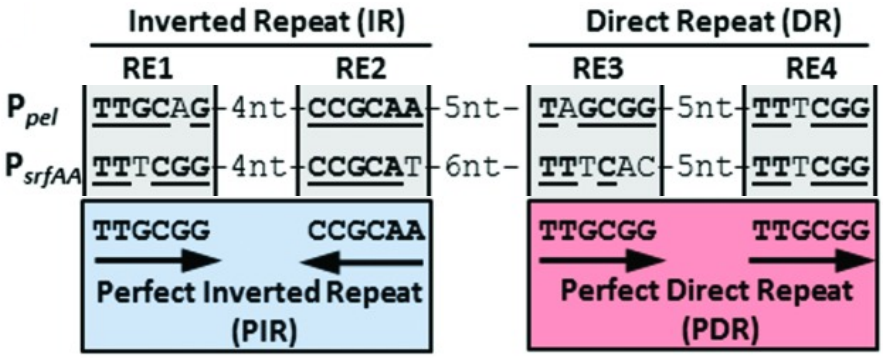

Figure 4.2 Sequence of the native ComA binding sites and the derived synthetic promoters [89]

4.2 Experimental Methods

4.2.1 Media

Table 4.1 LB medium composition

Compound	Amount (g/l)
Tryptone	10
NaCl	5
Yeast Extract	5

Note: LB agar was made by LB medium supplemented with 15 g/l Agar
Starch agar was made by LB agar supplemented with 10 g/l starch

Table 4.2 Composition of S7 medium

Compound	Stock conc.	Final conc.	Purchased Company
K2HPO4	1 M	3.075 mM	Sigma Aldrich
KH2PO4	1 M	1.925 mM	Sigma Aldrich
(NH4)2SO4	1 M	10 mM	Sigma Aldrich

Table 4.3 Composition of $S7_{50}$

Compound	Stock con.	Final conc.	Purchased Company
S7	100 %	80 %	Sigma Aldrich
MOPS	0.5 M (pH= 7)	50 mM	Sigma Aldrich
D-Glucose	20 %	1 %	Sigma Aldrich
Potassium L-Glutamate	5 %	0.1 %	Sigma Aldrich
L-Tryptophan	5 mg/ml	50 µg/ml	Sigma Aldrich
MnCl2	10 mM	50 µM	Sigma Aldrich
FeSO4	1 mM	5 µM	Sigma Aldrich
MgSO4	1 M	2 mM	Sigma Aldrich
Thiamine	1 mM	2 µM	Sigma Aldrich
ZnCl2	1 mM	1 µM	Sigma Aldrich
CaCl2	1 M	700 µM	Sigma Aldrich

4.2.2 Fluorescence Reporter Assays

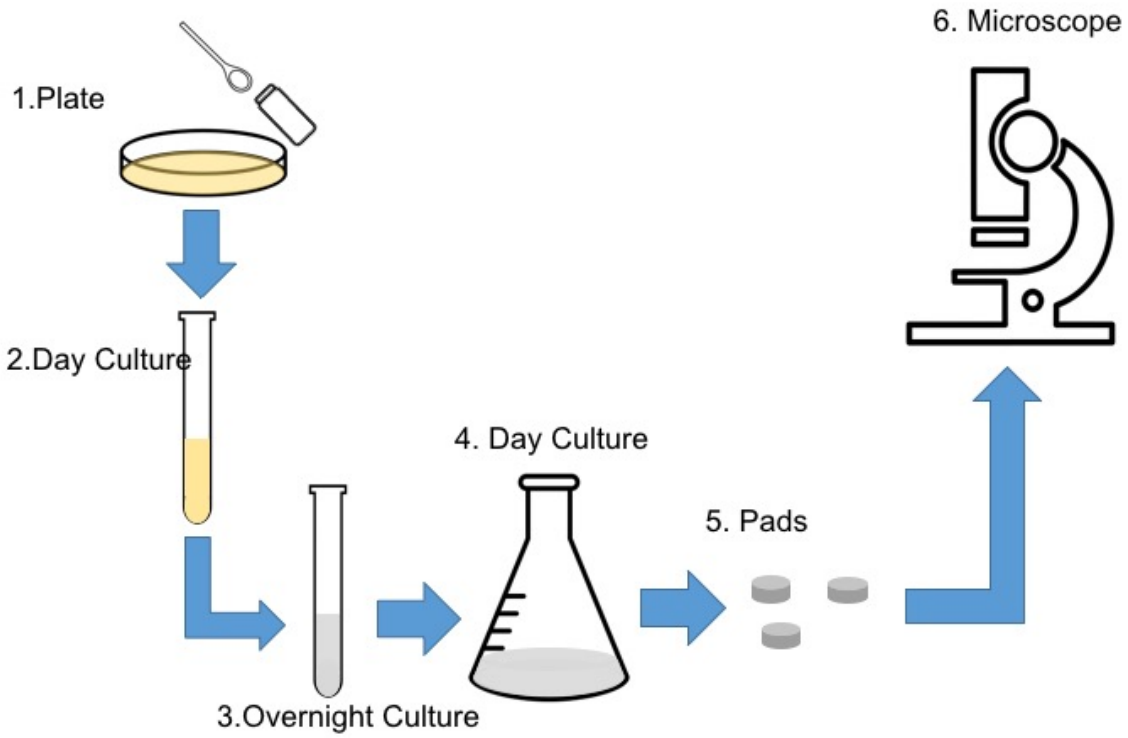

Figure 4.3 Experiment setup for Fluorescence Reporter Assays

4.2.3 Culture Growth Conditions

In order to prepare *B. subtilis* culture for fluorescence reporter assays, adopted protocol from ref [90] was implemented. First, desired *B. subtilis* strains were streaked on an agar plate with required antibiotics and were sequentially incubated for overnight (~17 hrs) at 37 ˚C. Following the overnight incubation, a single colony was picked with a micropipette tip and inoculated in 5 mL LB medium with necessary antibiotics for a day culture. The day culture was incubated at 37 ˚C and 180 rpm for 6 hours. The day culture cell suspension was used to start an overnight culture with 3 mL of $S7_{50}$ medium (see table for composition) and necessary antibiotics with a starting OD_{600} of 0.025. The overnight culture in $S7_{50}$ medium was incubated at 30 ˚C and 180 rpm for 18 hrs until thin layer of biofilm was visible and OD_{600} reached 8+/-1.5. In order to measure the OD_{600} of overnight culture, culture cell suspension was vigorously vortexed to break down the biofilm

and obtain homogeneous solution. All the bacteria culture up to this state were done in 16 mm diameter glass tubes. Finally, a fresh day culture was inoculated in 10 mL of $S7_{50}$ medium at 37 ˚C and 180 rpm with starting OD_{600} of 0.02. A day culture was inoculated in 100 mL glass flask and bacterial cell culture was harvested accordingly during the day culture. After harvesting the bacterial cell at desired day culture time or OD_{600}, cell culture suspension was centrifuged at 8000 g for 5 minute then the supernatant was removed and it was resuspended in the PBS. The washing step was done twice in total and the supernatant was resuspended at OD_{600} of 2 in PBS after the final wash.

4.2.4 Gel pads preparation

In order to run the *B. subtilis* fluorescence reporter assays, agarose gel pads which act as a substrate for bacterial cells were need to be prepared. Gel pads for fluorescence reporter assay consisted of 1% ultra-pure agarose in PBS. In each pad 2 µL of culture was uniformly spread.

4.2.5 Microscope Conditions

Fluorescence reporter assay microscope images were imaged with an Olympus 1X71 microscope (Olympus, Japan). The microscope was equipped with DeltaVision Elite Imaging System (Applied Precision, USA) and UPlanSApo 100x oil objective (Olympus, Japan) with Edge SCMOS camera (PCO Germany) was used for imaging. The filter and exposure settings listed in Table 4.4 was used otherwise stated. The microscope was set with C/YFP/mCh polychromic, imaging size of 512 x 512 and binning of 2 x 2 settings. During the imaging sessions, beam conditions and always Kohler was turned on.

Table 4.4 Fluorescence Microscope Setting

Channel	Filter	Trans. [%]	Exp. [sec]
Bright Field	POL / POL	32	0.025
Fluorescence	CFP / CFP	100	0.5
Fluorescence	YFP / YFP	100	0.3

4.2.3 Time-lapse Microscopy Assays

4.2.3.1 Microfluidic

For time-lapse microscopy assays, microfluidic plate from CellAsics was purchased and slightly modified recommended protocol provided by the company was followed to run the assays. Just to briefly describe the procedures, about 8 hours prior to running the assay, the microfluidic plate packaging was opened under the sterile environment and left on a lab bench at room temperature with the plate lid on until the next usage. This was done to release PDMS structures that may have stuck together from the possible mechanical stress applied during the vacuum sealing. Additional attempt to remove this stress was done by purging the plate according to the "B04Purge Protocol 050714" around one hour prior to loading the sample. The plate was made sure to be purged by checking under the microscope with the bright field and if not purged properly, purging was done multiple times. After purging was ensured, Pre-filled PBS from the manufacture was carefully aspirated from all channels and 100 µL of to be primed solution was put in each channels in-let well. Desired solutions were accordingly primed in each channel using the "B04 Prime and Devac Protocol 092614". After channels have been primed with the desired solution, 50 µl of the cell suspension (OD_{600} = 1) were filled in inlet of channel 8 and loaded with the manufactures provided protocol. The loading was done twice to make sure to trap enough cells in imaging area. During the time-lapse imaging, inlet solutions were stimulated at pressure of 6 psi which corresponds to a

flow rate of approximately 15 µl per hour. Depending on the assay duration stimulation inlet well was switched every 12 hours.

4.2.3.2 Microscope conditions

During the time-lapse microscopy assays, same microscopy to run the Fluorescence Reporter Assays was used. An Uplan SApo air 40x objective lens and the image size of 1024 by 1024 was set with the binning of 1 by 1. Auxiliary magnification was turned on for the time-lapse assays and image was recorded every 10 minutes with the below exposure setting. Relatively long exposure had to be used for fluorescence channels to obtain a signal that is stronger that the background noise raising from the PDMS structures.

Table 4.5 Fluorescence Microscope Setting for microfluidic experiments

Channel	Filter	Trans. [%]	Exp. [sec]
Bright Field	POL / POL	32	0.05
Fluorescence	CFP / CFP	100	2
Fluorescence	YFP / YFP	100	2

4.2.4 Fluorescence reporter assay analysis

Single cells from bright-field images were segmented by a customized software [91] and manually inspected. For each inspected cell, the mean fluorescence intensity, size and circularity were determined from the segmented area. The mean fluorescence intensity was calculated by subtracting the background fluorescence from the fluorescence intensity of the segmented area.

4.3 Results and discussion

4.3.1 Phenotypic heterogeneity

Analysis of cells with the the P*srf*-cfp reporter demonstrated that at the 4 hours of incubation (OD_{600} = 0.2), the distribution of cells expressing surfactin show bimodal as in the figure 4.4 (a). The two peaks at intensity of 60 and 180 clearly demonstrate the bimodal pattern. This pattern arises from two distinct subpopulations where cells in one population show higher expression of the reporter and the other subpopulation exhibiting little or no expression of the reporter. In figure 4.4 (c), a micrograph taken of the same field of cells illustrating subpopulations with higher expression and little expression of surfactin is presented. The presented image is an overlay of fluorescence and transmitted light images. Interesting observation from the populations leading to bimodality is that there are two different morphologies being observed. A group of cells with short cell body coexists with the long and elongated ones. By comparing surfactin intensity of the cells with the morphology, it was found out that the long and elongated ones are the weak intensity ones where short ones have high intensity. A correlation plot in which the circulation is on the Y-axis and CFP fluorescence intensity on the X-axis is shown in figure 4.4 (b). Each data point in a plot represents a single cell. The circularity is defined as These results indicate that at the time of sampling, *B. subtilis* strain 216 show a heterogeneity behavior in level of surfactin production depending on the morphology of the cells.

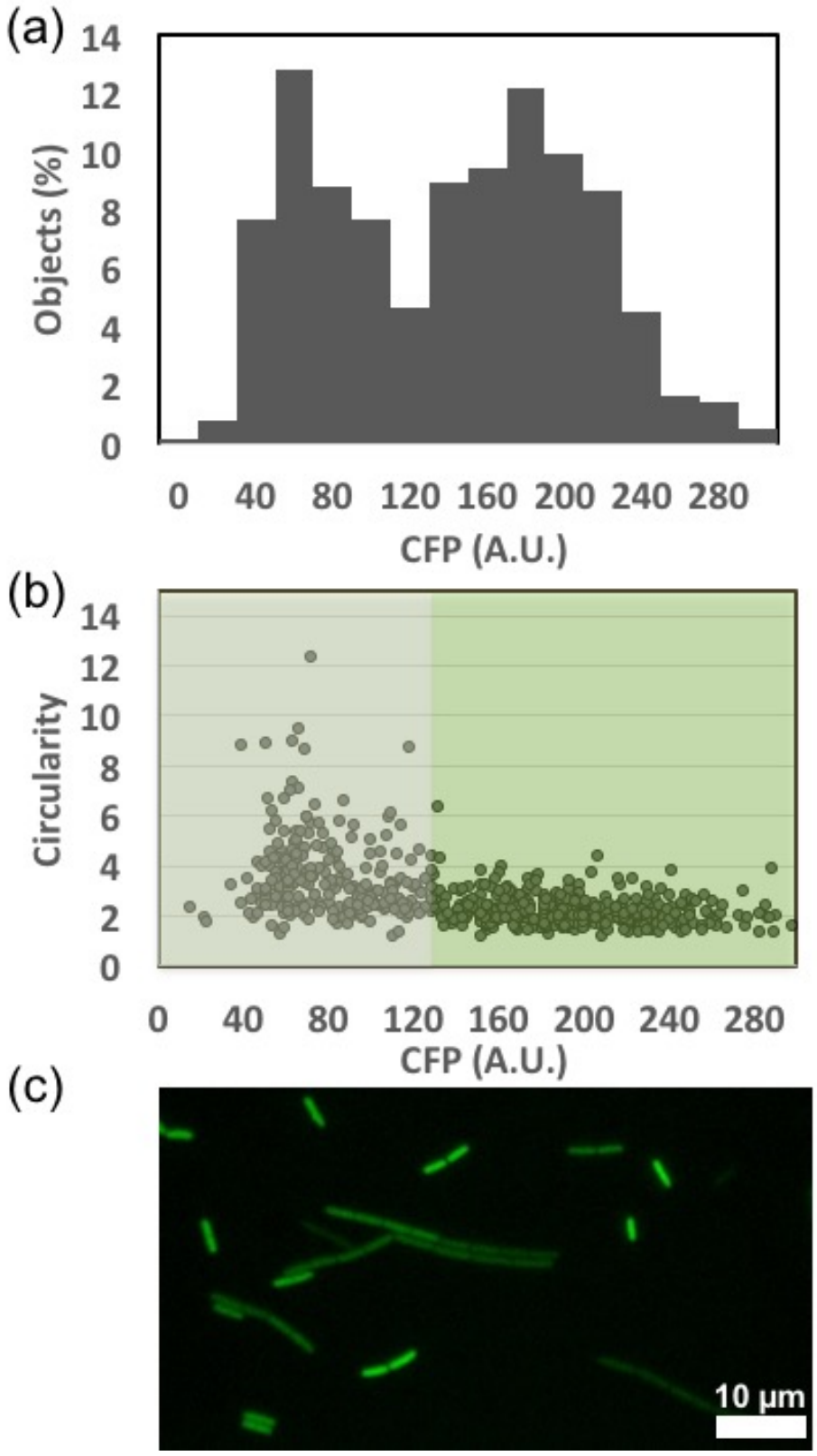

Figure 4.4 Heterogeneity observed in P*srf*

(a)P*srf* activity (b)Circularity and intensity correlation (c) Fluorescence image

4.3.2 Heterogeneity in Activity of ComA Natural Promoters

Another promoter regulated by comA, pectin lyases (*pel*) was monitored and analyzed at the same time as the surfactin promoter. A more detailed description of how dual color protein reporter structure was fused is described in the method section. By comparing the activity of these two promoters at the same time, a question whether a bimodal behavior rises from a shared labor or division of labor was looked at. As the name suggests, bacterial cells have not only been observed to act together but indeed overcome the challenges by diving the labor, in a manner different cell types specializing on distinct tasks. An example of such special behavior has been observed in *B. subtilis* by Gestel and et al, for a migration. [91] By comparing the intensity of two studied proteins which are known to be regulated by same transcription factor, one can found out whether different gene is expressed with the different morphology of the cells. For instance, if the studied *B. subtilis* strain actually do share labor at the sampling stage, one morphology would produce specific gene while the other one produce the other monitored gene. However, this was found to be not the case as shown in the Figure 4.5 (a). Figure 4.5 (a) plots a correlation between two studied genes where activity of P*srf* is plotted on the x-axis and while the activity of P*pel* is listed on the y-axis. Each point in a plot represents measurements from a single cell. The correlation factor of these two promoters were extremely high with 90%. Such high correlation factor strongly contrasts with the idea that shared labor occurs between P*srf* and P*pel*. To further support this, a micrograph of an overlay of two channels' fluorescence image is presented in Figure 4.5 (b). It is important to note that the Figure presented here is same field of cells as from the previous Figure 4.4 (c) except in this case both P*srf* and P*pel* fluorescence channels are presented where in Figure 4.4 (c), only P*srf* was shown. As already shown in Figure 4.4 (c). cells with short and small morphology show higher activity in both promoters and merged fluorescence images therefore show as bright yellow. In

comparison, long and elongated bacterial cells have weak intensity and hence shown as dim yellow. These results highly suggest that the both studied promoters are indeed regulated by common transcription factor ComA and the heterogeneity in gene expression is not occurring from the shared labor of *srf* and *pel*.

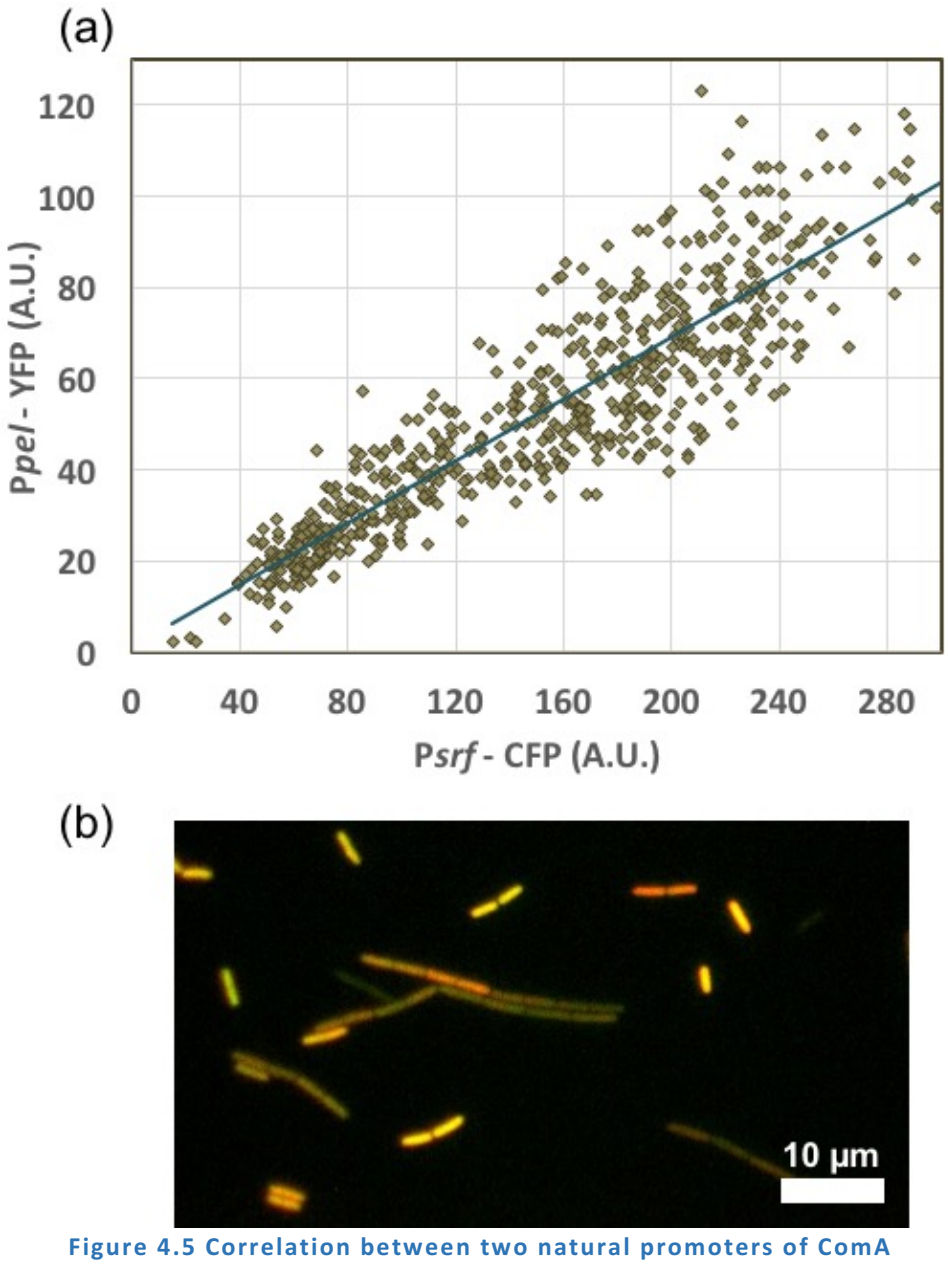

Figure 4.5 Correlation between two natural promoters of ComA

(a)Scatter plot showing the correlation between P*pel* and P*srf* (b) Fluorescence micrograph image showing both P*pel* and P*srf*

4.3.3 Natural promoter and synthetic promoter activity

In addition to *pel* and *srf* which are known to be comA specific target genes, two other genes were also monitored to confirm whether bimodality was only within genes regulated by comA or not. Another natural gene, *treP* protein was fused into *B. subtilis* with 216 background and harvested at the similar OD when different bacterial cell morphology and bimodality with natural promoters, surfactin and *pel* was observed. *treP* gene is known regulate carbohydrate utilization and unlike *pel* and *srf* genes it is not a target genes of comA. [92] Since the activity of *treP* gene was monitored with the *B. subtilis* 216 strain, different cell morphology was also observed as presented in Figure 4.6 (a) . However, the measured intensity of promoter activity showed unimodal peak (Figure 4.6 (a)) rather than the bimodal peaks in comparison to Figure 4.4 (a). The trend in promoter activity of *treP* continued to be unfluctuating and stayed as unimodal even after the heterogeneity in cell morphology disappeared. Similar experiment with a synthetic promoter was conducted. A synthetic promoter, PDR-PDR is a promoter designed in a lab as a consensus motif to have highest binding affinity to ComA. The more detailed description and previous experiments with this synthetic promoter is described in the ref [89]. In comparison to the *treP* promoter, synthetic promoter with higher binding affinity to ComA, indicated clear trend of bimodality among bacterial cells with different morphology as indicated in Figure 4.6 (b). As observed with natural promoters, P*pel* and P*srf*, short *B. subtilis* cells demonstrated higher promoter activity in comparison to low activity observed in long chain forming cells. From this results, a speculation that the observed heterogeneity in the activity of two monitored natural promoters in this study may be highly correlated to the activity of ComA. However, it is still not confirmed whether these phenomena are caused by other regulators that may affect P*srf* and P*pel* or just happening from the coincidence. These questions are difficult to answer with the scope of this study. However, a

question of what happens as the day culture continuous to grow under the same condition is answered in the upcoming part by harvesting the day culture at different time points and measuring the activity protein assay reporters each time.

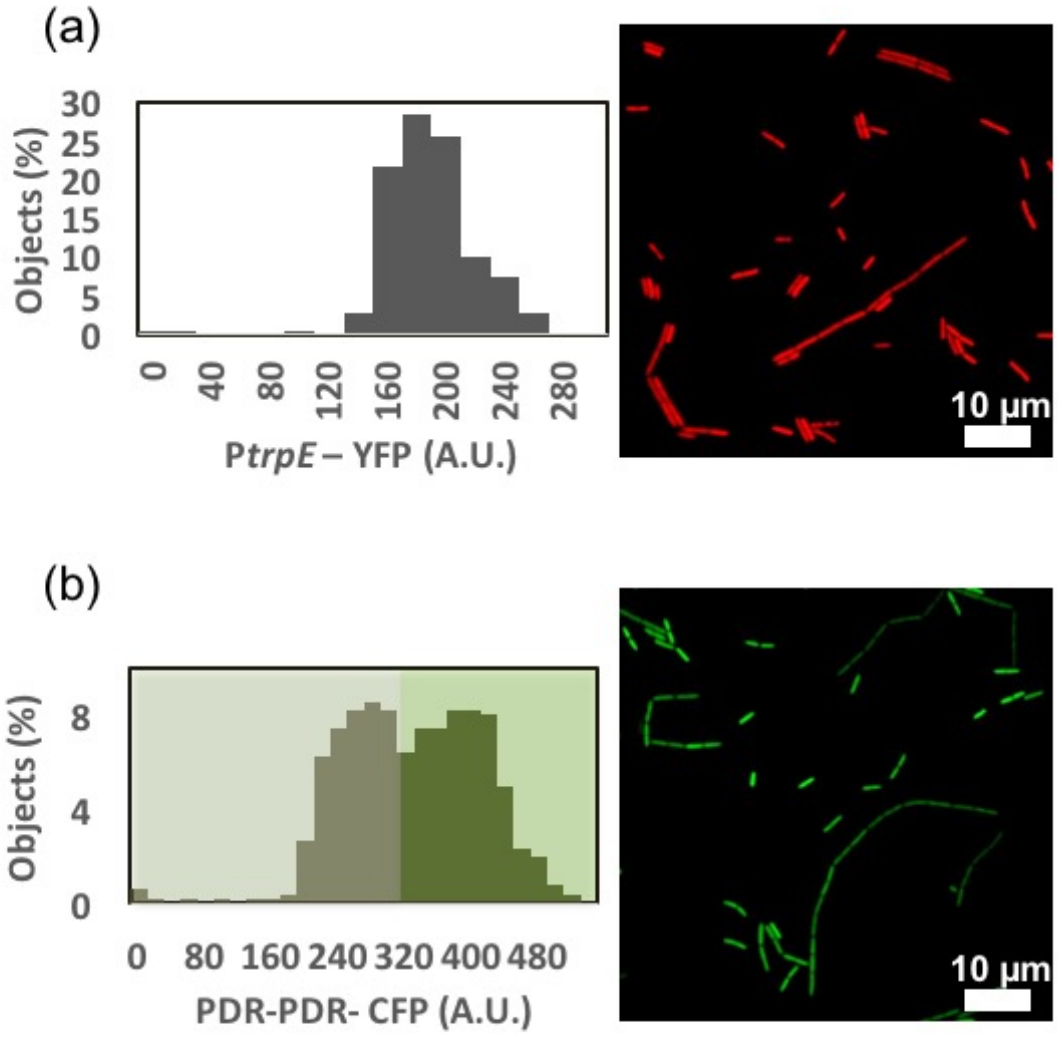

Figure 4.6 Natural and Snythetic promoter activity

(a)A natural promoter not regulated by ComA showing an unimodal peak (b)A synthetic promoter which has motif to match ComA showing a bimodal peak

4.3.4 Promoters activity over time

In total, day culture was harvested at four different time points and the measured OD_{600} at these four measured points with the respected incubated duration are shown in Figure 4.7 by a growth curve. The purpose of studying the life cycle of day culture was to examine the stability of the heterogeneity observed. The trend in growth curve indicate that the day culture was still going through a growth phase during the time of investigation.

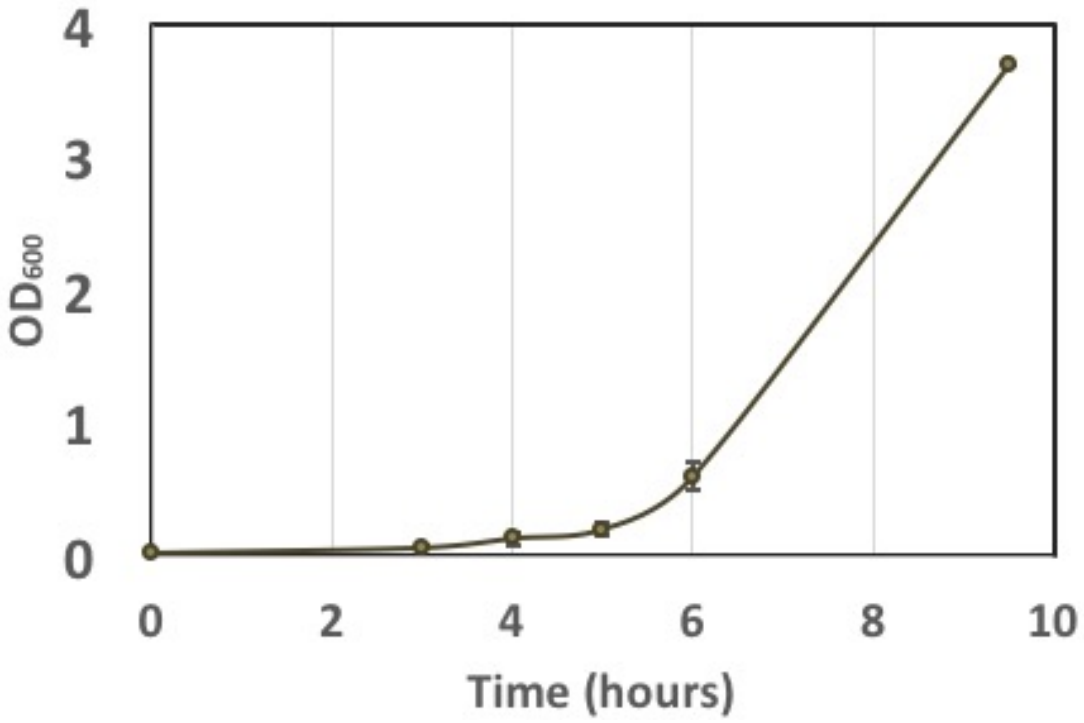

Figure 4.7 Growth curve with meeausred OD_{600} over the day culture

Table 4.6 Measured time points and the correlation coefficient factor between two studied natural promoters

Time Point	Incubation Hours	OD_{600}	Corr.Coef
1	3	0.06	0.91
2	4	0.14	0.90
3	5	0.2	0.90
4	9.5	3.7	0.69

In Figure 4.8, from the left of the figure, first histogram shows the measured intensity of the promoter of activity of P*srf*. Next to the fluorescence activity reporter assays, the correlation between the P*srf* and P*pel* is shown by the scatter plot in the middle figure. Lastly on the far right, bright field image merged with both fluorescence channels for each time point are presented. With a measured fluorescence activity of P*srf* shown on the left side of the Figure 4.8, The transparent grey area is there to represent a control sample with an empty vector. By having empty vector samples as controls, a background noise could be identified. For the CFP channel a peak at 50nm is identified as a background noise while YFP channel did not seem to have any noise raising from the background. At the first time point (OD_{600}=0.06), only short cells are present and both promoters are off with the minimal activity and having the mean intensity close to the background noises. Different bacterial cell morphology first occurred starting in 4 hours of incubation at the OD_{600} of 0.14 as shown at the time point 2 of Figure 4.8. With apparent of the two types of cell morphology, bimodality also emerged in both fluorescence channels. The correlation factor between two channels were calculated to be 0.9 indicating that the activity of two promoters are highly correlated and hence further pointing P*pel* and P*srf* are regulated by ComA or other possible common regulators. After one more addition hour of incubation from the second harvesting point, a third time point with total growth time of 5 hours (OD_{600}= 0.2) was imaged under the microscope and quantified as previously explained in the method section, the bacterial samples from the third time point had similar traits as the *B. subtilis* cells. Two distinct populations in terms of morphology, long ones and the short ones coexist in the same culture and the bimodality in protein expressions still existed except the gaps between two peaks became wider than the previous time point. From the merged micrograph of bright field and fluorescence channels, interesting phenome was observed in the long cells. At the time point 2 (OD_{600} = 0.14), the long cells did not have any

signs of breaking up or diving into small cells and seemed to be one single cell. In comparison, even though the elongated cells looked identical in bright field between time point 2 and 3, they demonstrated clear difference in the fluorescence channels. In the fluorescence channels, distinct diving lines were visible in the cells collected at the time point 3. The division lines indicate that the long chain cells would break off to become multiple short ones. At the last observed point, at time point 4 (OD_{600} = 9.5), long chain forming cells were no longer present and only short cells were present. The morphology of cells at time point 4 and point 1 are identical since there are only short ones in the population. However, compare to the point 1 where both studied promoters were off, P*pel* demonstrated clear induction at time point 4 as illustrated in Figure 4.8. The induction of P*pel* as the long cells break off to become single cells were also monitored with culture grown in a microfluidic device. Different from induced P*pel*, P*srf* showed no induction after time point 2 and the intensity exhibited decreasing trend over the time. A possible explanation for the heterogeneity with different morphology could be that the morphology of cells and the activity of ComA are somehow related. For instance, it could be that the at the phase of long chain cells, ComA of PS216 strain is inactive. Similar postulation has been reported by Lopez and et al, proclaiming that the long chain forming cells produce biofilm extracellular matrix once the production is triggered by the surfactin. [93] In this study, it is not certain whether the surfactin also leads to formation of extracellular matrix since the expression for extracellular matrix was not monitored. However, if this was indeed the same case for the strains used in this study as well, it could be that the long chains forming cells are coated by the biofilm extracellular matrix which could possibly hindering the activation of ComA. These biofilms coated long cells would become deaf to receiving signals from the environment and as a result express low signals in ComA regulated genes such as *pel* and *srf*. The coating may disappear as the long chain cells break off to

become short ones and again allow *B. subtilis* bacterial cells to react to ComA signal. It is not certain at this point whether pinching of the long chain cells to divide into multiple short ones contribute to the ComA pathway or not. More in depth study to elucidate the relationship between the morphology and heterogeneity in gene expression is required.

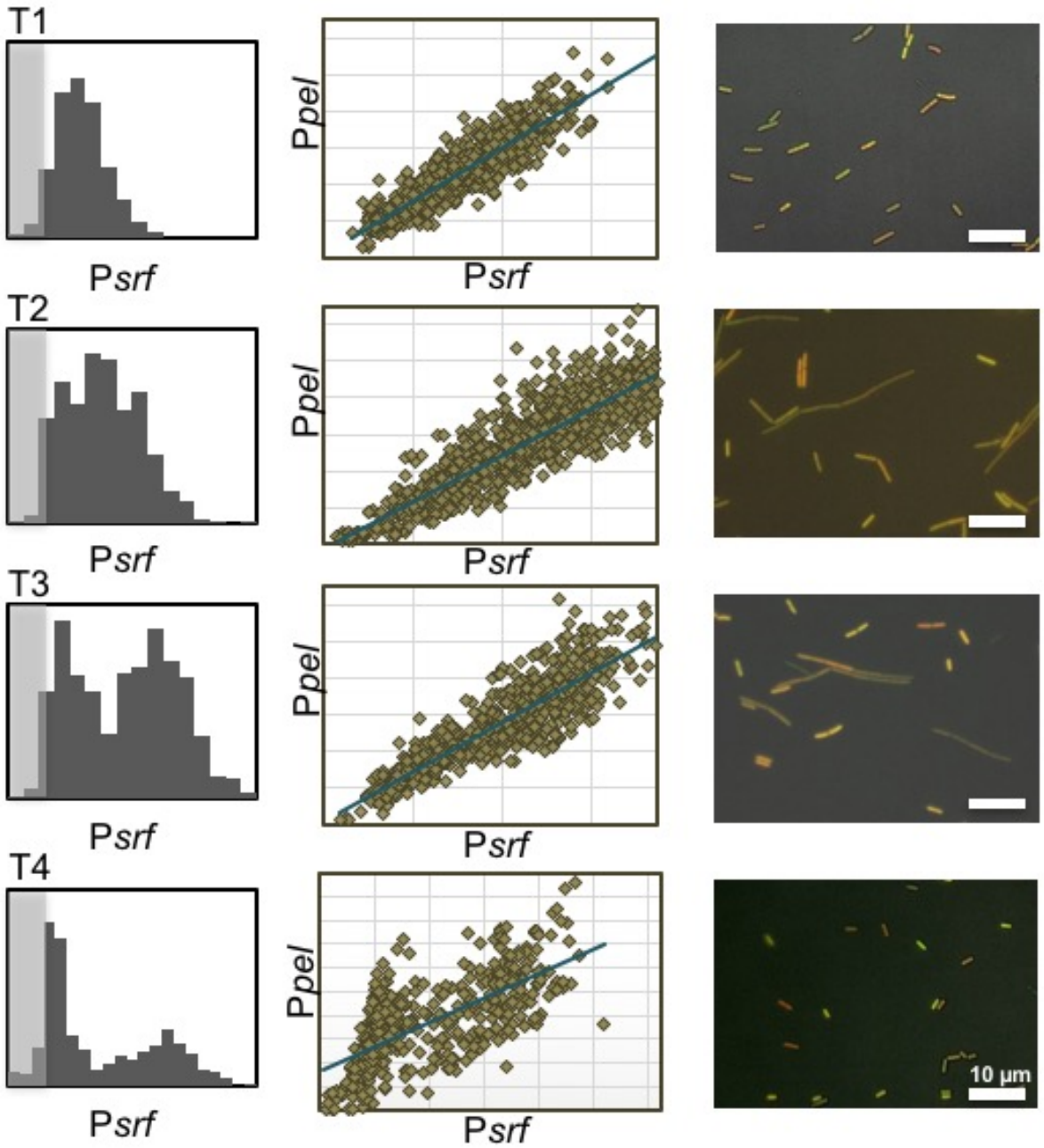

Figure 4.8 ComA regulated natural promoter activity over times series

4.4 Conclusion and recommendations

By constructing dual color protein assay of two natural promoters, P*pel* and Psrf which are responsible for pectin lyases and surfactin in respect, phenotypic heterogeneity in undomesticated *Bacillus subtilis* was observed. Two different types of morphology were seen where one type had short cell bodies with higher intensity in activity of both promoters and the other type with long cell bodies. The elongated cells distinguishably had low intensity in both analyzed natural promoters. Interesting phenomena of elongated cells breaking off to become multiple short cells were observed. During the division of chain forming ones, the P*pel* activity induced in contrast to the activity of the P*srf* which shut off after the certain point. Despite the fact that the both P*srf* and P*pel* are known to be regulated by the same transcription factor, it is unsure of the behind reason for such heterogeneity behaviour at this point of the study.

In order to further develop the study, it is recommended to study the activity of the biofilm extracellular matrix production to figure out the if the biofilm indeed inhibits the activity of ComA regulation or not. In terms of the experiments, it is suggested to repeat the experiments until enough sample population for both morphologies are obtained to conduct the statistical analysis. More optimized time lapse experiments are encouraged as well. For the microfluidic time lapse experiments, the fluorescence intensity could not be measured to the constantly changing background signal. The background noise for CFP channel was even higher and only the YFP channel could be used to visually analyze the growth behaviour of the samples. It is proposed to optimize fluorescence proteins to minimize the background noise or use other fluorescence proteins that might lead to less noise.

Chapter 5. Conclusions and Future Research Directions

Single cell isolation, application and analysis have been implemented in this study for engineering applications and studying regulation of gene expressions. Bacteria are ubiquitous and easier to grow and more durable than other widely used Eukaryotic cells. Throughout the first two projects, where single *S. aurues* cells been utilized for capturing nanoparticles and engineering with other magnetic particles, bacterial cells demonstrated outstanding adhesion property, ability to survive through harsh condition. In the last project, single bacterial cell analysis has illustrated phenotypic heterogeneity in wild type *B. subtilis* cells. Three individual projects with a common theme of utilizing single bacterium cell have been presented here and have succeeded for each purpose of the project. In the below section, the purpose of each projects, achieved results and the future research directions for each project is outlined.

In the Chapter 2, two different types of nanospheres have been successfully encapsulated in metal nanopillars. The results demonstrated that the opening top shape and dimensions of metal structures affect the capturing rate of both nanopillars and the sealing rate of bacterial cells. The highest filling and trapping rate of 85 % or higher was achieved with polystyrene spheres and hollow shaped pillars. In addition to demonstrating the possibility of capturing nanoparticles with live cells, a durability of capping was shown by exposing the adhered cells to the electron beam produced by the scanning electron microscope. As a result, rupture in cells were observed and this seemed to be depending on the adhering site of the bacterial cells. In order to carry the project one step forward, it is recommended to try different bacterial cells with different morphologies to verify whether higher success rate can be obtained. Rupturing cells and taking out the particles filled inside the hollow metal structures should be investigated since it would provide unique properties that other capping mechanisms may not. Lastly, the benefit of having a front slit with

C-shape structures should also be maximized. A front opening with a size of less than captured nanoparticles enable filled nanoparticles to interact with its surrounding while still being remained captured and this benefit should be tested.

In the following chapter, Chapter 3, same bacterial cells studied in Chapter 2 have been successfully patterned in an organized matter and engineered with magnetic nanoparticles. The presented method successfully achieves a highly ordered array of single *S. aureus* cells without any artificial changes in the surfaces. Unlike pre-existing methods, the present method achieves the goal of isolating and patterning submicron bacterial cells on the gold metal substrate by simple photoresist template, without any surface modification or binding agents. Different types of magnetic particles including gold and iron oxide have been engineering with the patterned *S. aureus* bacterial cells. The succeeding result in engineering interface between the bacterial cell and layers of charged particles demonstrate that the bacterial cell wall properties have been maintained during the isolation and the usage of presented technique for further developing microsystems. Developed technique in this thesis should be further investigated and incorporated to isolate other dimensions of bacterial cells by changing the dimensions of the template. In addition, experiments should be conducted to fabricate 3D structures of engineered bacterial cells with magnetic particles by overfilling the template. The 3D structures may provide to be a basic building blocks for the microsystems.

Different from the previous two chapters, last chapter analyzes single cells to study the behaviour of gene expression in the culture. In this study, another gram-positive bacterial cells called *B. subtilis* have been monitored over their growth state. Two natural promoters, P*pel* and P*srf* promoters were mainly monitored by fusing them with fluorescence proteins. These two natural promoters are known to be regulated by a common transcription factor called ComA. In contrast

to the common idea that the studies gens would behave the same due the same transcription factor, they illustrated heterogeneity behaviour in terms of the activity. More interestingly, the heterogeneity in gene expression was found out be correlating with the morphology of the cells. For both ComA dependent promoters, long cells showed less activity in promoters while the short cells demonstrated higher intensity of the proteins. The reason behind such interesting phenomena still remains to be inconclusive due to the depth of study conducted here. A simple postulation could be made that the observed heterogeneity may be related to the activity of ComA since the heterogeneity was not observed in the other natural promoter which is not regulated by ComA. In comparison, identical observation to the natural ComA target genes were seen in the synthetic promoter designed to consensus with ComA and hence strengthening the argument that the ComA related may be the underlying mechanism for the phenotypic heterogeneity. The presented result here has just begun to find an interesting path and the roads should be extended and further investigated. It is advisable to repeat the experiments shown here at least several times to obtain the enough data set to conduct a statistical analysis. Despite the fact that the presented experiments were done several times, the observed sampled population between two different morphology of cells were not controllable which may have led to undesirable biases. In addition, more well designed time-lapse studies in microfluidic devices are recommended. The time-lapse movies in the present thesis could not be analyzed due to the high intensity caused by the material of the device and hence the other fluorescence proteins need to be used for microfluidic device experiments or change in the material for microfluidic device is recommended.

Bibliography

[1] Alberts, B., Wilson, J., & Hunt, T. (2008). Molecular biology of the cell. New York: Garland Science.

[2] Bartholomew, J. W., & Mittwer, T. THE GRAM STAIN. Bacteriological Reviews, 1952; 16(1), 1–29.

[3] Jahed Z, Lin P, Seo BB, et al. Responses of Staphylococcus aureus bacterial cells to nanocrystalline nickel nanostructures. Biomaterials. 2014;35(14):4249 4254.

[4] J. Gu, P.Z. Chen, B.B. Seo, J.M. Jardin, M.S. Verma, Z. Jahed, et al., Adhesion characteristics of Staphylococcus aureus bacterial cells on funnel-shaped palladium – cobalt alloy nanostructures, 2016;11(7):480-489.

[5] Desbiens J, Bergeron B, Patry M, et al. Polystyrene nanoparticles doped with a luminescent europium complex. J Colloid Interface Sci. 2012;376(1):12 19.

[6] Fehrmann C, Jurk K, Bertling A, et al. Role for the fibrinogen-binding proteins coagulase and Efb in the *Staphylococcus aureus-Candida* interaction. Int J Med Microbiol. 2013; 303(5):230 238.

[7] Kahraman AS, Gumusderlioglu M, Tuncel A. Cellular interactions of monodisperse poly (GDMA) latex particles-containing DMAEM brushes. Colloids Surfaces A. 2011; 384(1 3):90 97.

[8] Lokhande AB, Mishra S, Kulkarni RD, et al. Influence of different viscosity grade ethylcellulose polymers on encapsulation and in vitro release study of drug loaded nanoparticles. J Pharm Res. 2013;7(5):414 420.

[9] Oslakovic C,Cedervall T,LinseS,etal.Polystyrenenanoparticlesaffectingbloodcoagulation. Nanomedicine. 2012;8(6):981 986.

[10] Yoo HS, Kim TG, Park TG. Surface-functionalized electrospun nanofibers for tissue engineering and drug delivery. Adv Drug Deliv Rev. 2009;61(12):1033 1042.

[11] MadisonR,MacklisJD,ThiesC.Latexnanospheredeliverysystem(LNDS):novelnanometer-sized carriers of fluorescent dyes and active agents selectively target neuronal subpopulations via uptake and retrograde transport. Brain Res. 1990;522(1):90 98.

[12] OhJK,LeeDI,ParkJM.Biopolymer-basedmicrogels/nanogelsfordrugdeliveryapplications. Prog Polymer Sci. 2009;34(12):1261 1282.

[13] Oh JK, Drumright R, Siegwart DJ, et al. The development of microgels/nanogels for drug delivery applications. Prog Polymer Sci. 2008;33(4):448 477.

[14] Orive G, Santos E, Pedraz JL ,et al.Application of cell encapsulation for controlled delivery of biological therapeutics. Adv Drug Deliv Rev. 2014;67 68:3 14.

[15] Pichot C. Surface-functionalized latexes for biotechnological applications. Curr Opin Colloid Interface Sci. 2004;9(3 4):213 221.

[16] Liu Y, Li W, Lao F, et al. Intracellular dynamics of cationic and anionic polystyrene nanoparticles without direct interaction with mitotic spindle and chromosomes. Biomaterials. 2011;32(32):8291 8303.

[17] Pellach M, Goldshtein J, Ziv-Polat O, et al. Functionalised, photostable, fluorescent polystyrene nanoparticles of narrow size-distribution. J Photochem Photobiol A.

2012;228(1) 60 67.
[18] Venkataraman S, Hedrick JL, Ong ZY, et al. The effects of polymeric nanostructure shape on drug delivery. Adv Drug Deliv Rev. 2011;63(14 15):1228 1246.
[19] Tian Q, Zhang Z, Yang L, et al. Encapsulation of SnO2 nanoparticles into hollow TiO2 nanowires as high performance anode materials for lithium ion batteries. J Power Sources. 2014;253:9 16.
[20] An J, Wang D, Luo Q, et al. Antimicrobial active silver nanoparticles and silver/polystyrene core-shell nanoparticles prepared in room-temperature ionic liquid. Mater Sci Eng C 2009; 29(6):1984 1989.
[21] Ding X, Zhao J, Liu Y, et al. Silica nanoparticles encapsulated by polystyrene via surface grafting and in situ emulsion polymerization. Mater Lett. 2004;58(25):3126 3130.
[22] Ladj R, Bitar A, Eissa MM, et al. Polymer encapsulation of inorganic nanoparticles for biomedical applications. Int J Pharm. 2013;458(1):230 241.
[23] Park S, Lee S, Jeong S, et al. Nanosilver colloids-filled photonic crystal arrays for photoluminescence enhancement. Nanoscale Res Lett. 2010;5:1590 1595.
[24] Dow W-P, Shen S-P, Lu C-W, et al. Through silicon vias and holes metallization by Cu nanoparticles coating and Cu electrodeposition [Abstract #2005]. 218th Electrochemical Society Meeting; 2010 Oct 10 15, Las Vegas, NV.
[25] Arens S, Schlegel U, Printzen G, et al. Influence of materials for fixation implants on local infection in rabbits. J Bone Joint Surg [Br]. 1996;78-B:647 651.
[26] Campoccia D, Baldassarri L, Pirini V, et al. Molecular epidemiology of Staphylococcus aureus from implant orthopaedic infections: ribotypes, agr polymorphism, leukocidal toxins and antibiotic resistance. Biomaterials. 2008;29(30):4108 4116.
[27] Ercan B, Kummer KM, Tarquinio KM, et al. Decreased Staphylococcus aureus biofilm growth on anodized nanotubular titanium and the effect of electrical stimulation. Acta Biomater. 2011;7(7):3003 3012.
[28] Gristina AG. Biomaterial-centered adhesion versus infection: microbial tissue integration. Science. 1987;237(4822):1588 1595.
[29] Harris LG, Richards RG. Staphylococci and implant surfaces: a review. Injury. 2006;37(Suppl 2):S3 14.
[30] Moran E, Byren I, Atkins BL. The diagnosis and management of prosthetic joint infections. J Antimicrob Chemother. 2010;65(Suppl 3):iii45 iii54.
[31] Rochford ETJ, Poulsson HC, Salavarrieta Varela J, et al. Bacterial adhesion to orthopaedic implant materials and a novel oxygen plasma modified PEEK surface. Colloids Surfaces B. 2014;113:213 222.
[32] Truong VK, Lapovok R, Estrin YS, et al. The influence of nano-scale surface roughness on bacterial adhesion to ultrafine-grained titanium. Biomaterials. 2010;31(13):3674 3683.
[33] Wang X, Wang G, Liang J, et al. Staphylococcus aureus adhesion to different implant surface coatings : An in vitro study. Surface Coating Technol. 2009;203(22):3454 3458.
[34] Wu Y, Zitelli JP,TenHuisen KS,et al. Differential response of Staphylococci and osteoblaststo varying titanium surface roughness. Biomaterials. 2011;32(4):951 960.
[35] Burek MJ, Greer JR. Fabrication and microstructure control of nanoscale mechanical testing specimens via electron beam lithography and electroplating. Nano Lett. 2010;10(1):69 76.
[36] Burek MJ, Jin S, Leung MC, et al. Grain boundary effects on the mechanical properties of

bismuth nanostructures. Acta Mater. 2011;59(11):4709–4718.
[37] Seo BB, Jahed Z, Burek MJ, et al. Influence of grain size on the strength size dependence exhibited by sub-micron scale nickel structures with complex cross-sectional geometries. Mater Sci Eng A. 2014;596:275-284.
[38] Rashidi AM, Amadeh A. Effect of electroplating parameters on microstructure of nanocrystalline nckel coatings. J Mater Sci Technol. 2010;26(1):82–86.
[39] Costello C, Kreft JU, Thomas CM and Mendes PM. Protein Nanoarrays for High-Resolution Patterning of Bacteria on Gold Surfaces. Methods Mol Biol. 2011; 790:191–200
[40] Rawson FJ, Yeung CL, Jackson SK, Mendes PM. Tailoring 3D single-walled carbon nanotubes anchored to indium tin oxide for natural cellular uptake and intracellular sensing. Nano Lett. 2013; 13:1–8
[41] Costello CM, Yeung CL, Rawson FJ, Mendes PM. Application of nanotechnology to control bacterial adhesion and patterning on material surfaces. J Exp Nanosci. 2012; 7:634–651
[42] Whitesides GM, Ostuni E, Jiang X, Ingber DE. Soft Lithography in Biology and Biochemistry. Annu Rev Biomed Eng. 2001; 3:335–73
[43] Karreman RJ, Dague E, Gaboriaud F, Quilès F, Duval JFL, Lindsey GG. The stress response protein Hsp12p increases the flexibility of the yeast Saccharomyces cerevisiae cell wall. Biochim Biophys Acta. 2007; 1774:131–137
[44] Dague E, Delcorte A, Latgé J-P, Dufrêne YF. Combined use of atomic force microscopy, X-ray photoelectron spectroscopy, and secondary ion mass spectrometry for cell surface analysis. Langmuir. 2008; 24:2955–2959
[45] Francius G, Tesson B, Dague E, Martin-Jézéquel V, Dufrêne YF. Nanostructure and nanomechanics of live Phaeodactylum tricornutum morphotypes. Environ Microbiol. 2008; 10:1344–1356
[46] Xu L, Robert L, Ouyang Q, Taddei F, Chen Y, Lindner AB, Baigl D. Microcontact printing of living bacteria arrays with cellular resolution. Nano Lett. 2007; 7:2068–2072
[47] Weibel DB, Lee A, Mayer M, Brady SF, Bruzewicz D, Yang J, Diluzio WR, Clardy J, Whitesides GM. Bacterial printing press that regenerates its Ink: Contact-printing bacteria using hydrogel stamps. Langmuir. 2005; 21:6436–6442
[48] Cerf A, Cau J-C, Vieu C. Controlled assembly of bacteria on chemical patterns using soft lithography. Colloids Surf B Biointerfaces. 2008; 65:285–291
[49] Takayama S, Ostuni E, LeDuc P, Naruse K, Ingber DE, Whitesides GM. Selective chemical treatment of cellular microdomains using multiple laminar streams. Chem Biol. 2003; 10:123–130
[50] Merrin J, Leibler S, Chuang JS. Printing multistrain bacterial patterns with a piezoelectric inkjet printer. PLoS One. 2007; doi: 10.1371/journal.pone.0000663
[51] Eun YJ, Weibel DB. Fabrication of microbial biofilm arrays by geometric control of cell adhesion. Langmuir. 2009; 25:4643–4654

[52] Ingham C, Bomer J, Sprenkels A, van den Berg A, de Vos W, van Hylckama Vlieg J. High-resolution microcontact printing and transfer of massive arrays of microorganisms on planar and compartmentalized nanoporous aluminium oxide. Lab Chip. 2010; 10:1410–1416
[53] Cerf A, Cau J-C, Vieu C. Controlled assembly of bacteria on chemical patterns using soft lithography. Colloids Surf B Biointerfaces. 2008; 65:285–291
[54] Gristina a G, Hobgood CD, Webb LX, Myrvik QN. Adhesive colonization of biomaterials and antibiotic resistance. Biomaterials. 1987; 8:423–426
[55] Francois P, Schrenzel J, Stoerman-Chopard C, Favre H, Herrmann M, Foster TJ, Lew DP, Vaudaux P. Identification of plasma proteins adsorbed on hemodialysis tubing that promote Staphylococcus aureus adhesion. J Lab Clin Med. 2000; 135:32–42
[56] Harris LG, Meredith DO, Eschbach L, Richards RG. Staphylococcus aureus adhesion to standard micro-rough and electropolished implant materials. J Mater Sci Mater Med. 2007; 18:1151–1156
[57] Barth E, Myrvik QM, Wagner W, Gristina AG. In vitro and in vivo comparative colonization of Staphylococcus aureus and Staphylococcus epidermidis on orthopaedic implant materials. Biomaterials. 1989; 10:325–328
[58] Oga M, Sugioka Y, Hobgood CD, Gristina AG, Myrvik QN. Surgical biomaterials and differential colonization by Staphylococcus epidermidis. Biomaterials. 1988; 9:285–289
[59] Verma MS, Chen PZ, Jones L, Gu FX. "Chemical nose" for the visual identification of emerging ocular pathogens using gold nanostars. Biosens Bioelectron. 2014; 61:386–390
[60] Verma MS, Chen PZ, Jones L, Gu FX. Branching and size of CTAB-coated gold nanostars control the colorimetric detection of bacteria. RSC Adv. 2014; 4:10660
[61] Ozaki M, Kratohvil S, Matijević E. Formation of monodispersed spindle-type hematite particles. *J. Colloid Interface Sci.* 1984; 102, 146–151.
[62] Stober W, Fink A, Bohn E. Controlled Growth of Monodisperse Silica Spheres in Micron Size Range. J. Colloid Interface Sci. 1968; 26, 62–69.
[63] Leshuk T, Everett P, Krishnakumar H, Wong K, Linley S, Gu FX. Mesoporous Magnetically Recyclable Photocatalysts for Water Treatment. J. Nanosci. Nanotechnol. 2013; 13, 3127–3132.
[64] Caruso F, Caruso RA, Möhwald H. Nanoengineering of Inorganic and Hybrid Hollow Spheres by Colloidal Templating. Science 1998; 282, 1111–1114.
[65] Caruso F, Lichtenfeld H, Donath E, Möhwald H. Investigation of Electrostatic Interactions in Polyelectrolyte Multilayer Films: Binding of Anionic Fluorescent Probes to Layers Assembled onto Colloids. Macromolecules 1999; 32, 2317–2328.
[66] Silhavy TJ, Kahne D, Walker S. The Bacterial Cell Envelope. Cold Spring Harb Perspect Biol. 2010; 2, 16
[67] Berlot S, Aissaoui Z, Pavon-Djavid G, Belleney J, Jozefowicz M, Hélary G, Migonney V. Biomimetic poly(methyl methacrylate)-based terpolymers: Modulation of bacterial adhesion effect. Biomacromolecules. 2002; 3, 63–68

[68] Anagnostou F, Debet A, Pavon-Djavid G, Goudaby Z, Hélary G, Migonney V. Osteoblast functions on functionalized PMMA-based polymers exhibiting Staphylococcus aureus adhesion inhibition. Biomaterials. 2006; 27, 3912–3919
[69] Sung YJ, Suk HJ, Sung HY, Li T, Poo H, Kim MG. Novel antibody/gold nanoparticle/magnetic nanoparticle nanocomposites for immunomagnetic separation and rapid colorimetric detection of Staphylococcus aureus in milk. Biosens Bioelectron. 2013; 43, 432–439
[70] Chang Y-C, Yang C-Y, Sun R-L, Cheng Y-F, Kao W-C, Yang P-C. Rapid single cell detection of Staphylococcus aureus by aptamer-conjugated gold nanoparticles. Sci Rep, 2013; 3, 1863
[71] Seo B.B, Chen P.Z, Jahed Z, Mohammad R.K., Gu F.X. Tsui T.Y. Trapping polystyrene and latex nanospheres inside hollow nanostructures using Staphylococcus aureus cells, 2015; 37–41
[72] D.R. Zeigler, S. Rodriguez, B. Chevreux, A. Muffler, T. Albert, R. Bai, et al., The Origins of 168 , W23 , and Other Bacillus subtilis Legacy Strains, 2008; 190, 6983–6995
[73] D. Higgins, J. Dworkin, Recent progress in Bacillus subtilis sporulation, FEMS Microbiol Rev. 36, 2012; 131–148
[74] Durrett R, Miras M, Mirouze N, Narechania A, Mandic-Mulec I, Dubnau D, Genome sequence of the *Bacillus subtilis* biofilm-forming transformable strain PS216. Genome Announc. 2013; 1
[75] Ackermann M, A functional perspective on phenotypic heterogeneity in microorganisms, Nat. Publ. 2015; 13, 497–508
[76] Chung J.D, Stephanopoulos G, Ireton K, Grossman, A.D. 1994. Gene expression in single cells of *Bacillus subtilis*: Evidence that a threshold mechanism controls the initiation of sporulation. J. Bacteriol. 1994; 176, 1977–1984
[77] González-Pastor, J.E., Hobbs, E.C., Losick, R. Cannibalism by sporulating bacteria. Science. 2003; 301. 510–513
[78] Fujita, M., González-Pastor, J.E., Losick, R. High- and low-threshold genes in the Spo0A regulon of *Bacillus subtilis*. J. Bacteriol. 2005; 187. 1357–1368
[79] Kearns D.B., Losick R, Cell population heterogeneity during growth of *Bacillus subtilis*, Genes Dev. 2005; 19. 3083–3094
[80] Shaligram N.S, Singhal R.S, Surfactin – A Review on Biosynthesis , Fermentation , Purification and Applications, Food Technol. Biotechnol. 2010; 48. 119–134
[81] Marin-Rodriguez, M. C., John O, and Graham B.S , Pectate Lyases, Cell Wall Degradation and Fruit Softening. Journal of Experimental Botany. 2002; 53. 2115-119
[82] Miller M.B, Bassler B.L, Quorum Sensing in Bacteria, Annu. Rev. Microbiol. 2001; 55. 165–199
[83] Bassler B.L, Losick R, Bacterially Speaking, Cell. 2006; 125. 237–246.
[84] Comella N, Grossman A.D, Conservation of genes and processes controlled by the quorum response in bacteria: Characterization of genes controlled by the quorum-sensing transcription factor ComA in Bacillus subtilis, Mol. Microbiol. 2005; 57. 1159–1174.
[85] Okada M, Sato I, Cho S.J, Iwata H, Nishio T, Dubnau D, et al, Structure of the *Bacillus subtilis* quorum-sensing peptide pheromone ComX., Nat. Chem. Biol. 2005; 23–24.

[86] Core L, M. Perego, TPR-mediated interaction of RapC with ComA inhibits response regulator-DNA binding for competence development in Bacillus subtilis, Mol. Microbiol. 2003; 49. 1509–1522
[87] Nakano M.M, Zuber P, Mutational analysis of the regulatory region of the srfA operon in Bacillus subtilis., J. Bacteriol. 1993; 175. 3188–3191
[88] Guillen N, Weinrauch Y, Dubnau D.A, Cloning and characterization of the regulatory Bacillus subtilis competence genes comA and comB, J. Bacteriol. 1989; 171. 5354–5361
[89] Wolf D, Rippa V, Mobarec J.C, Sauer P, Adlung L, Kolb P, et al., The quorum-sensing regulator ComA from Bacillus subtilis activates transcription using topologically distinct DNA motifs, Nucleic Acids Res. 2015; 44. 2160–2172
[90] Trauth S, Bischofs I.B, Ectopic integration vectors for generating fluorescent promoter fusions in Bacillus subtilis with minimal dark noise, PLoS One. 2014; 9. 5
[91] Bischofs IB, Hug JA, Liu AW, Wolf DM, Arkin AP, Complexity in bacterial cell-cell communication: quorum signal integration and subpopulation signaling in the Bacillus subtilis phosphorelay. Proc Natl Acad Sci U S A. 2009; 106. 6459–6464
[92] Gestel J, Vlamakis H, Kolter R, From Cell Differentiation to Cell Collectives: *Bacillus subtilis* Uses Division of Labor to Migrate, PLoS Biol. 2015; 13. 1–29
[93] Schöck F, Dahl M.K, Expression of the tre operon of Bacillus subtilis 168 is regulated by the repressor TreR, J. Bacteriol. 1996; 178. 4576–4581
[94] López D, Vlamakis H, Losick R, Kolter R, Paracrine signaling in a bacterium, Genes Dev. 2009; 23. 1631–1638